

# Gravitino or Axino Dark Matter with Reheat Temperature as high as $10^{16}$ GeV

Raymond T. Co<sup>1,2</sup>, Francesco D'Eramo<sup>3,4</sup> and Lawrence J. Hall<sup>1,2</sup>

<sup>1</sup>*Berkeley Center for Theoretical Physics, Department of Physics,  
University of California, Berkeley, CA 94720, USA*

<sup>2</sup>*Theoretical Physics Group, Lawrence Berkeley National Laboratory, Berkeley, CA 94720, USA*

<sup>3</sup>*Department of Physics, University of California Santa Cruz, Santa Cruz, CA 95064, USA*

<sup>4</sup>*Santa Cruz Institute for Particle Physics, Santa Cruz, CA 95064, USA*

## Abstract

A new scheme for LSP dark matter is introduced and studied in theories of TeV supersymmetry with a QCD axion,  $a$ , and a high reheat temperature after inflation,  $T_R$ . A large overproduction of axinos ( $\tilde{a}$ ) and gravitinos ( $\tilde{G}$ ) from scattering at  $T_R$ , and from freeze-in at the TeV scale, is diluted by the late decay of a saxion condensate that arises from inflation. The two lightest superpartners are  $\tilde{a}$ , with mass of order the TeV scale, and  $\tilde{G}$  with mass  $m_{3/2}$  anywhere between the keV and TeV scales, depending on the mediation scale of supersymmetry breaking. Dark matter contains both warm and cold components: for  $\tilde{G}$  LSP the warm component arises from  $\tilde{a} \rightarrow \tilde{G}a$ , while for  $\tilde{a}$  LSP the warm component arises from  $\tilde{G} \rightarrow \tilde{a}a$ . The free-streaming scale for the warm component is predicted to be of order 1 Mpc, independent of  $m_{3/2}$  in the case of  $\tilde{G}$  LSP.  $T_R$  can be as high as  $10^{16}$  GeV, for any value of  $m_{3/2}$ . The PQ symmetry breaking scale  $V_{PQ}$  depends on  $T_R$  and  $m_{3/2}$  and can be anywhere in the range  $(10^{10} - 10^{16})$  GeV. Detailed predictions are made for the decay length of the neutralino LSP decaying to  $(\tilde{a}/\tilde{G} + h/Z)$ , which is in the range of  $(10^{-1} - 10^6)$ m over much of parameter space. For an axion misalignment angle of order unity, the axion contribution to dark matter is sub-dominant, except when  $V_{PQ}$  approaches  $10^{16}$  GeV. A scheme with neutralino dark matter is also mentioned, arising from  $\tilde{a}$  freeze-in, dilution from the saxion condensate, and decays to neutralinos.

# Contents

<b>1</b>	<b>Introduction</b>	<b>2</b>
<b>2</b>	<b>Saxion Cosmology</b>	<b>6</b>
<b>3</b>	<b>Axino and Gravitino Production</b>	<b>12</b>
<b>4</b>	<b>Axino and Gravitino as the Lightest Superpartners</b>	<b>17</b>
<b>5</b>	<b>Neutralino LSP from Axino Freeze-In</b>	<b>32</b>
<b>A</b>	<b>Axion Supermultiplet Interactions</b>	<b>33</b>
<b>B</b>	<b>Decay Widths</b>	<b>37</b>
<b>C</b>	<b>Free Streaming of Warm DM Component</b>	<b>41</b>

## 1 Introduction

Perturbative theories with supersymmetry broken at the TeV scale are well-motivated by the hierarchy problem, even if they do not completely solve it, and lead to Higgs boson masses in the region discovered at the LHC. Dark matter could be the lightest superpartner (LSP), cosmologically produced by the freeze-out mechanism. On the other hand, the strong CP problem is elegantly solved by introducing a Peccei-Quinn (PQ) symmetry [1, 2] broken at scale  $V_{PQ}$ ,<sup>1</sup> leading to a light axion degree of freedom  $a$  [3, 4] that relaxes the  $CP$ -violating phase  $\bar{\theta}$  to zero. In this case dark matter could be axions produced by the misalignment mechanism, with  $V_{PQ}$  of order  $10^{12}$  GeV a motivated possibility.

However, the cosmology of these two leading candidates for dark matter, LSPs and axions, is changed enormously in theories that have *both* weak scale supersymmetry and axions. The axion,  $a$ , must be promoted to a superfield

$$A = \frac{s + ia}{\sqrt{2}} + \sqrt{2}\theta\tilde{a} + \theta^2 F \quad (1.1)$$

and the saxion,  $s$ , and the axino,  $\tilde{a}$ , both play central roles in cosmology.

In this work, for reasons discussed below, we focus on DFSZ theories [5, 6], where the PQ symmetry forbids the  $\mu$  term of the minimal supersymmetric standard model (MSSM). At the scale  $V_{PQ}$ , PQ breaking induces the  $\mu$  term as well as a coupling of the axion supermultiplet with the MSSM Higgs superfields

$$W_{\text{DFSZ}} = \mu H_u H_d + q_\mu \frac{\mu}{V_{PQ}} A H_u H_d + \dots, \quad (1.2)$$

---

<sup>1</sup>In this work we use the PQ breaking scale  $V_{PQ}$  defined in Eq. (A.2), instead of the axion decay constant  $f_a$ . These two quantities are connected by a color anomaly coefficient, as shown explicitly in Eq. (A.5) of App. A.

with  $q_\mu$  a model dependent parameter defined in App. A. The superpotential cubic coupling is responsible for axino production in the early universe [7], either through decays or inverse decays of charginos and neutralinos,  $\tilde{\chi} \rightarrow \tilde{a}$ . This axino production by the freeze-in (FI) mechanism is IR dominated [8], namely most of the axinos are produced at temperatures around the TeV scale. Depending on the fermion content of the PQ breaking sector, a large abundance of axinos can also be produced in the UV, at the temperature  $T_R$  at the end of inflationary reheating [9], analogous to UV production of gravitinos [10].

In order to make this distinction sharper, we define two different types of theories:

**DFSZ<sub>0</sub>:** the heaviest colored fermion carrying PQ charge is the top quark, so the only source for axino production is the IR dominated freeze-in;

**DFSZ<sub>+</sub>:** there is at least one heavy (of order  $V_{PQ}$ ) colored fermion carrying PQ charge, and thus we also have UV dominated production at  $T_R$  from gluino scattering off quarks and gluons.

In DFSZ<sub>0</sub>, an IR contribution to axino production via scattering also arises from the supersymmetrized  $aG\tilde{G}$  operator generated when the top quark is integrated out [11], but it is suppressed compared to the one from decays and we neglect it. In theories with a low gravitino mass, the decay of neutralinos can also populate gravitinos by the FI mechanism but we find this contribution sub-dominant to the ones mentioned above.

In the absence of a saxion condensate, UV production of both axinos and gravitinos puts a very powerful bound on  $T_R$  [12]. This is illustrated in Fig. 1 both for DFSZ<sub>0</sub> (left panel) and DFSZ<sub>+</sub> (right panel) for gravitino LSP and other superpartners at the TeV scale. Contours that yield the DM relic density are shown in the  $(V_{PQ}, T_R)$  plane for four values of the gravitino masses. Even for a gravitino with a weak scale mass, the reheat temperature after inflation is strongly bounded,  $T_R \lesssim 10^8$  GeV. Thus LSP dark matter is typically overproduced in the absence of a saxion condensate, unless  $V_{PQ}$  is very large and  $T_R$  is very low. However, if  $V_{PQ}$  is very large so that axino freeze-in is significantly suppressed, the universe is typically overclosed by axions, unless a low value of the axion misalignment angle is selected by an anthropic requirement.

Saxion cosmology can greatly change this conclusion. Axion theories typically have a domain wall problem, which we assume is solved by breaking the PQ symmetry before inflation, and not restoring it afterwards. We define the saxion field so that today the saxion vev is zero. During inflation supersymmetry breaking yields a potential for the saxion, displacing the vev away from today's value. Depending on the sign of the quadratic term, the vacuum value  $s_I$  is either  $V_{PQ}$  or of order the cutoff of the field theory,  $M_* \gg V_{PQ}$  [13].<sup>2</sup> If  $s_I \gtrsim 10^{13}$  GeV or  $s_I \sim M_*$ , this saxion condensate comes to dominates the energy density of the universe, producing an early matter-dominated (MD) era. When the saxion condensate decays, large entropy is created that has a key effect on both LSP and axion contributions to dark matter. The conventional picture of dark matter survives only for the restricted case of  $s_I \sim V_{PQ} \lesssim 10^{13}$  GeV, when the saxion condensate never dominates, allowing the usual favorite cases of LSP freeze-out or axion misalignment with  $V_{PQ} \sim 10^{12}$  GeV. However, as we have already mentioned, this case of low

---

<sup>2</sup>The possibility  $s_I = 0$  requires a special symmetry structure that we do not consider in this paper.

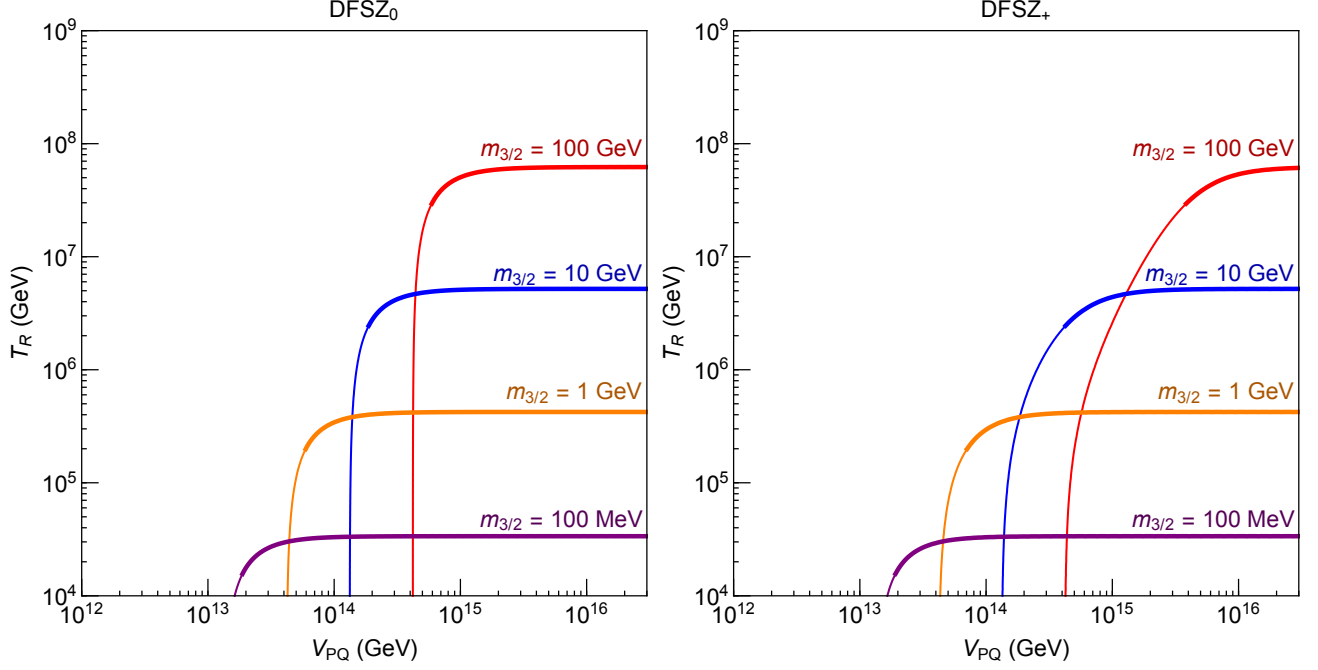


Figure 1: Contours yielding the observed dark matter abundance for a gravitino LSP in the absence of a saxion condensate for DFSZ<sub>0</sub> (left panel) DFSZ<sub>+</sub> (right panel), with  $M_1 = M_2/2 = \mu = 1$  TeV,  $\tan \beta = 2$  and  $q_\mu = 2$ . The axino mass is in the range  $m_{3/2} \lesssim m_{\tilde{a}} \lesssim \mu$ . For UV production in DFSZ<sub>+</sub> we fix  $N_{DW} = 6$ . Vertical lines correspond to axino freeze-in via decays  $\tilde{\chi} \rightarrow \tilde{a}$ , whereas horizontal lines correspond to UV gravitino production at  $T_R$ . The thick (thin) portions of the lines correspond to a freeze-in contribution smaller (larger) than 50%.

$V_{PQ}$  has a serious cosmological problem. Even if we choose  $T_R$  low enough to suppress UV production, there is still the IR contribution from freeze-in, which cannot be suppressed unless we select  $T_R$  below the superpartner mass scale. Hence we consider larger  $s_I$ , giving a saxion condensate MD era that has important consequences for dark matter abundance.

In KSVZ [14, 15] axion theories the MSSM  $\mu$  term is not forbidden by PQ symmetry and the axion multiplet does not couple to the Higgs superfields. Thus the saxion typically has a large decay branching ratio to axions and the decay of the saxion condensate gives an axion contribution to dark radiation that is excluded [16]. Hence we focus on DFSZ theories.

In our scheme the dominant saxion decay is to pairs of Higgs,  $W$  or  $Z$  bosons, giving a very low reheat temperature of the saxion<sup>3</sup>  $T_{Rs}$ ; for example,  $T_{Rs} \sim \text{GeV} - \text{MeV}$  for  $V_{PQ} \sim (10^{13} - 10^{16})$  GeV, respectively. The decay of the saxion condensate has crucially important implications for dark matter:

- The LSP abundance from freeze-out is greatly diluted [17, 18]. The freeze-out mechanism can only give the observed dark matter abundance if it first overproduces LSPs that are

<sup>3</sup>We define  $T_R$  and  $T_{Rs}$  as the reheat temperatures after inflation and saxion decays, respectively.

then diluted. This could happen by raising superpartners well above the TeV scale.

- For  $V_{PQ} > 10^{13}$  GeV, the entropy is released after the axion condensate starts to oscillate, diluting misalignment axions. For a misalignment angle of order unity, the value of  $f_a$  needed for axion dark matter is raised from  $\sim 10^{12}$  GeV to  $\sim 10^{15}$  GeV [19], suggesting the possibility that PQ and grand unified gauge symmetries are broken together [20].
- The large abundances of gravitinos and axinos produced at  $T_R$ , and of axinos produced by freeze-in at the TeV scale, are diluted by saxion decays, greatly weakening the constraints of Fig. 1 and allowing much higher  $T_R$  and lower  $V_{PQ}$ .
- If kinematically allowed, the saxion condensate leads to a late production of superpartners, and therefore LSPs, via such decays  $s \rightarrow \tilde{a}\tilde{a}, \tilde{a}\tilde{G}, \tilde{\chi}\tilde{\chi}$ .

Given these crucial effects of the saxion condensate, what are the leading candidates and production mechanisms for dark matter? Misalignment axions with  $V_{PQ}$  the scale of grand unification becomes one attractive option [20]. In this paper we consider the LSP possibility.

We work in a generic framework of TeV scale supersymmetry, taking the saxion and axino masses of order the TeV scale, as well as all other superpartners except, perhaps, the gravitino which could be much lighter. Freeze-out gives too low an abundance for a typical TeV-scale superpartner spectrum, although a bino-like LSP is a possibility providing the condensate is not too large. On the other hand, if  $s$  decays to superpartners are kinematically allowed, the late decay of the condensate typically overproduces LSP dark matter. Hence we assume these decays are kinematically forbidden and focus on two mechanisms for LSP production: IR freeze-in of axinos from neutralinos and charginos,  $\tilde{\chi} \rightarrow \tilde{a}$ , and UV scattering at  $T_R$  producing axinos and gravitinos,  $g\tilde{g} \rightarrow \tilde{a}, \tilde{G}$ . We consider three possibilities for the LSP:  $\tilde{a}, \tilde{G}$  and  $\tilde{\chi}$ , and perform a systematic analysis for the dark matter abundance over a very wide range of  $T_R$  and  $V_{PQ}$ , identifying regions of both cold and warm dark matter. A key feature of our work is to connect the dark matter cosmology with displaced vertex signals, arising from superpartner production and decay to gravitinos [21] and axinos [22], at the LHC and future colliders.

There is a considerable literature on the effects of a saxion condensate on LSP abundances. The gravitino and axino problems were solved by the decay of a saxion condensate in Ref. [23], which also considered the possibility of gravitino dark matter from inflaton decay. This was further developed by identifying PQ-breaking fields as the waterfall fields of a hybrid inflation model with vevs of order  $10^{15}$  GeV [24]. An alternative solution to the gravitino problem involved a very light, keV axino [25, 26]. In other work a saxion condensate was used to obtain a PQ breaking scale as large as the unification scale in theories with axino or neutralino LSP [27], and further work considered mixed axino/neutralino dark matter [28].

We describe the saxion condensate MD era in Sec. 2, by identifying the characteristic temperatures associated to this epoch and giving analytical expressions for them. The production mechanisms for axino and gravitino are discussed in detail in Sec. 3, where we account for the dilution for the saxion condensate and give numerical results for the yields  $Y_{\tilde{a}}$  and  $Y_{3/2}$  as a function of  $V_{PQ}$ . In Sec. 4, we study the cases of axino and gravitino LSP for two classes of SUSY spectra: high scale (i.e. “gravity”) and low scale (i.e. “gauge”) mediation, analyzed in

Sec. 4.1 and 4.2, respectively. In both cases we have the possibility that LSP dark matter is warm, with free streaming length as illustrated in Fig. 7. It is intriguing that this result can be consistent with Lyman- $\alpha$  forest observations while at the same time solving issues with cosmological structures at small scales. LSP relic density results for high scale mediation are shown in Figs. 8 and 10, whereas the analogous results for low scale are in Figs. 12 and 14. A remarkable signal of our framework, which holds regardless of the mediation scale, is displaced events at colliders, with decay lengths predicted in Figs. 9, 11, 13, 15 and 16. Neutralino LSPs are discussed in Sec. 5. The freeze-out contribution is highly suppressed by the saxion condensate, so that the main source of neutralino is through production and decay of axinos and gravitinos. We supplement our work by Appendices with useful results employed in our analysis.

## 2 Saxion Cosmology

Inflationary dynamics sets the initial conditions for the saxion condensate, typically displacing it by an amount  $s_I$  from the minimum today. After inflation ends, Hubble friction keeps the saxion field fixed until the universe expands and cools sufficiently that  $3H \sim m_s$ , with  $m_s$  the saxion mass, when the saxion condensate oscillates around its minimum. The energy density stored in such oscillations red-shifts like non-relativistic matter, thus slower than radiation, and eventually dominates the energy budget.

The specific temperature where saxion oscillations begin is crucial for the evolution of the saxion condensate. In particular, we identify two main regimes according to the size of the reheat temperature after inflation

$$T_R \begin{matrix} > \\ < \end{matrix} \sqrt{m_s M_{Pl}} \sim \mathcal{O}(10^{10}) \text{ GeV} \quad (2.1)$$

and describe the cosmologies separately. In the case where  $T_R \gtrsim 10^{10}$  GeV, saxion oscillations start during the radiation-dominated era after inflationary reheating has ended, while in the case where  $T_R \lesssim 10^{10}$  GeV, they start during inflationary reheating.

In addition to the saxion condensate that arises from inflationary dynamics, the saxion can also be generated from the thermal processes such as the scattering of the heavy colored fermions with PQ charges in the DFSZ<sub>+</sub> theories. This contribution is sub-dominant when  $s_I > 10^{13-14}$  GeV. For  $s_I < 10^{13-14}$  GeV, we find that the extra thermal saxions still fail to provide the dilution necessary for the overproduced axinos from UV scattering. Therefore, this thermal contribution of saxions is never relevant in the parameter space of interest.

### 2.1 High reheat temperature after inflation: $T_R \gtrsim 10^{10}$ GeV

Saxion oscillations begin when the radiation bath has a temperature

$$T_{osc} = \left( \frac{10}{\pi^2 g_*(T_{osc})} \right)^{\frac{1}{4}} \sqrt{m_s M_{Pl}} , \quad (2.2)$$

where we introduce the effective number of relativistic degrees of freedom in the thermal bath  $g_*(T)$  and the reduced Planck's mass  $M_{\text{Pl}} = 2.4 \times 10^{18}$  GeV. The onset of saxion oscillation happens during an early Radiation Dominated era (RD'). The energy stored in saxion oscillations red-shifts with the scale factor  $a$  as  $a^{-3}$ , namely with the same behavior of non-relativistic matter. If the condensate is long-lived enough, it eventually takes over the radiation energy and the universe enters an early matter-dominated (MD) era at a temperature  $T_M$ . This characteristic temperature is found by imposing that the saxion and the radiation bath equally contribute to the energy density, or in other words by solving the equation

$$m_s^2 s_I^2 \frac{g_*(T_M)}{g_*(T_{\text{osc}})} \left( \frac{T_M}{T_{\text{osc}}} \right)^3 = \frac{\pi^2}{30} g_*(T_M) T_M^4, \quad (2.3)$$

where we use the conservation of the total entropy to properly red-shift the saxion energy. Only for the purpose of an analytical estimate, we set  $g_*(T_{\text{osc}}) = g_*(T_M) = 228.75$ , corresponding to the full MSSM field content, giving

$$T_M \simeq 10 \text{ TeV} \left( \frac{m_s}{1 \text{ TeV}} \right)^{\frac{1}{2}} \left( \frac{s_I}{10^{15} \text{ GeV}} \right)^2. \quad (2.4)$$

This early MD era consists of two distinct phases, as detailed in Refs. [7, 20]. In the beginning, the radiation energy density is dominated by the red-shifted initial component. We dub this initial part an adiabatic matter-dominated ( $\text{MD}_A$ ) era. However, radiation coming from saxion visible decays red-shifts slower and in the end accounts for most of the radiation present in the universe. Once the contribution from saxion decays dominates, at a temperature  $T_{NA}$ , we enter a non-adiabatic matter-dominated ( $\text{MD}_{NA}$ ) era, where the total entropy is not conserved. At temperatures below  $T_{NA}$ , saxion decays reheat the universe and a large amount of entropy is released. Finally, most of the saxions decay when the Hubble parameter is of the order of the saxion decay width,  $H \sim \Gamma_s$ . This is the beginning of the last phase of a radiation-dominated universe (RD), which starts when the radiation bath has the reheat temperature  $T_{Rs}$ .

We assume that saxion decays to R-odd neutralinos and charginos are kinematically forbidden, and that decays to axions are sub-dominant. The saxion width is thus dominated by decays to MSSM Higgs bosons and longitudinal electroweak gauge bosons. We use the expression in Eq. (B.8) for the saxion visible width, valid in the decoupling limit and for large  $\tan \beta$ . The transition from  $\text{MD}_A$  to  $\text{MD}_{NA}$  occurs at temperature

$$T_{NA} \simeq 0.2 \text{ GeV} q_\mu^{\frac{4}{5}} \left( \frac{\mathcal{D}}{4} \right)^{\frac{2}{5}} \left( \frac{\mu}{1 \text{ TeV}} \right)^{\frac{13}{10}} \left( \frac{\mu}{m_s} \right)^{\frac{3}{10}} \left( \frac{s_I}{V_{PQ}} \right)^{\frac{2}{5}} \left( \frac{10^{15} \text{ GeV}}{V_{PQ}} \right)^{\frac{2}{5}}, \quad (2.5)$$

where we used  $g_*(T_{Rs}) = 10.75$  and  $\mathcal{D}$  denotes the number of final states kinematically accessible ( $\mathcal{D} = 4$  for SM and  $\mathcal{D} = 8$  for the full MSSM). The non-adiabatic era ends once the saxion condensate decays, reheating the universe at the temperature

$$T_{Rs} \simeq 10 \text{ MeV} q_\mu \left( \frac{10.75}{g_*(T_{Rs})} \right)^{\frac{1}{4}} \left( \frac{\mathcal{D}}{4} \right)^{\frac{1}{2}} \left( \frac{\mu}{1 \text{ TeV}} \right)^{\frac{3}{2}} \left( \frac{\mu}{m_s} \right)^{\frac{1}{2}} \left( \frac{10^{15} \text{ GeV}}{V_{PQ}} \right). \quad (2.6)$$

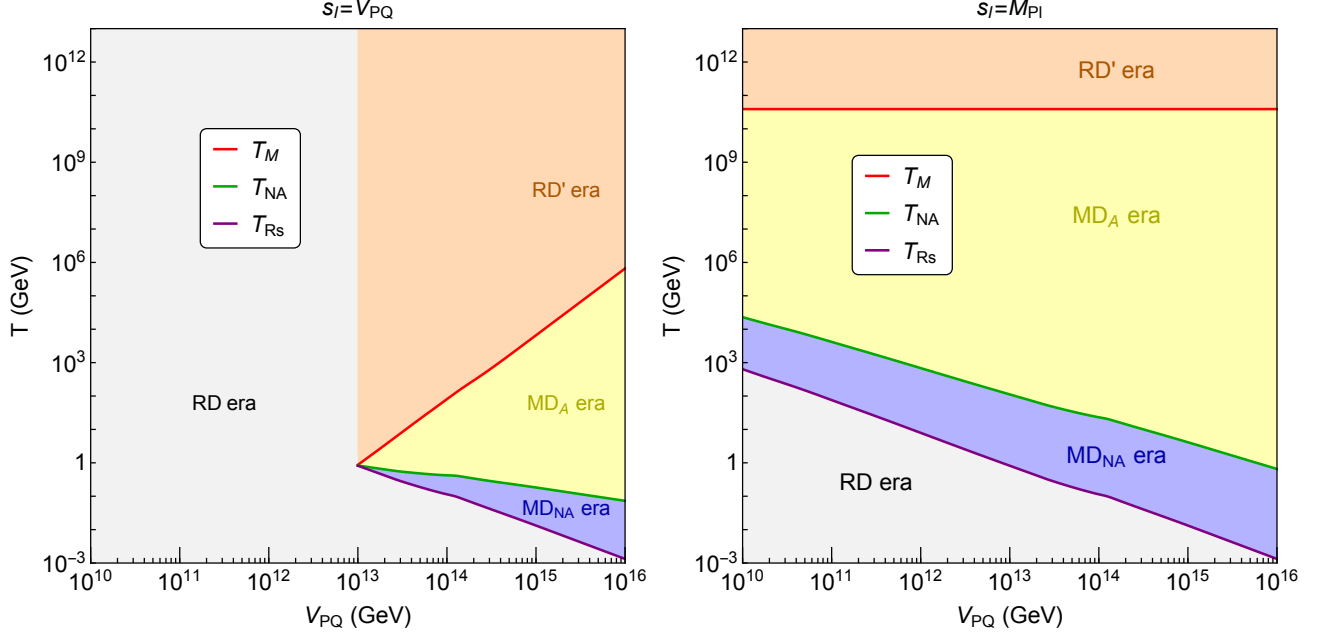


Figure 2: Cosmological eras for  $T_R \geq 10^{10}$  GeV.  $T_M$ ,  $T_{NA}$  and  $T_{Rs}$  as functions of  $V_{PQ}$  with  $s_I = V_{PQ}$  ( $M_{Pl}$ ) in the left (right) panel,  $\mu = m_s = 1$  TeV,  $q_\mu = 1$ , and  $\mathcal{D} = 4$ . The RD', MD<sub>A</sub>, MD<sub>NA</sub>, RD eras are individually shaded.

The three characteristic temperatures  $T_M$ ,  $T_{NA}$  and  $T_{Rs}$  are shown in Fig. 2. We plot their values as a function of  $V_{PQ}$  for two different initial conditions:  $s_I = V_{PQ}$  (left panel) and  $s_I = M_{Pl}$  (right panel). In the first case, we notice that for  $V_{PQ} \lesssim 10^{13}$  GeV there is no matter dominated era. For such low values of  $V_{PQ}$ , the initial saxion energy density is not enough to overtake radiation before it decays. Thus,  $T_M$  and  $T_{NA}$  are not defined and there is no significant entropy production at  $T_{Rs}$ . We define  $V_{PQ}^{(c)}$  this critical value of  $V_{PQ}$ , corresponding to the intersection of the three lines in the left panel of Fig. 2.

A physically meaningful and useful quantity is the amount of entropy released by saxion decays during the reheating process. We quantify this by introducing the dilution factor  $D(T_i)$ , defined as the ratio of the entropy after saxion decays to that at an initial temperature  $T_i$

$$D(T_i) \equiv \frac{S_{Rs}}{S_i} = \frac{g_*(T_{Rs})T_{Rs}^3}{g_*(T_i)T_i^3} \left( \frac{a_{Rs}}{a_i} \right)^3. \quad (2.7)$$

We interpret  $T_i$  as the temperature when the dark matter is produced, e.g. freeze-in temperature. In the MD<sub>NA</sub> era, we make use of the scaling  $a^3 \propto T^{-8}$ , whereas in the MD<sub>A</sub> and RD eras,  $a^3 \propto T^{-3}$ . With  $T_{NA}^5 \simeq T_M T_{Rs}^4$ , we obtain the following dilution factor

$$D(T_i) \approx \begin{cases} \frac{T_M}{T_{Rs}} & T_i \geq T_{NA} \\ \left( \frac{T_i}{T_{Rs}} \right)^5 & T_{NA} \geq T_i \geq T_{Rs}. \end{cases} \quad (2.8)$$



We can thus find  $D$  from Eqs. (2.4) and (2.6)

$$D(T_i) \simeq \begin{cases} 10^6 \left(\frac{2}{q_\mu}\right) \left(\frac{4}{\mathcal{D}}\right)^{\frac{1}{2}} \left(\frac{1 \text{ TeV}}{\mu}\right) \left(\frac{m_s}{\mu}\right) \left(\frac{s_I}{V_{PQ}}\right)^2 \left(\frac{V_{PQ}}{10^{15} \text{ GeV}}\right)^3 & T_i \geq T_{NA} \\ 10^5 q_\mu^{-5} \left(\frac{T_i}{100 \text{ MeV}}\right)^5 \left(\frac{4}{\mathcal{D}}\right)^{\frac{5}{2}} \left(\frac{1 \text{ TeV}}{\mu}\right)^{\frac{15}{2}} \left(\frac{m_s}{\mu}\right)^{\frac{5}{2}} \left(\frac{V_{PQ}}{10^{15} \text{ GeV}}\right)^5 & T_{NA} \geq T_i \geq T_{Rs}. \end{cases} \quad (2.9)$$

The dilution factor is extremely large for the initial condition  $s_I = M_{Pl}$ , ranging from  $10^9$  to  $10^{15}$  as  $V_{PQ}$  increases from  $10^{10}$  GeV to  $10^{16}$  GeV. On the other hand, the  $s_I = V_{PQ}$  case has a much small dilution, varying from 1 to  $10^9$  as  $V_{PQ}$  increases from  $10^{13}$  GeV to  $10^{16}$  GeV. Each comoving number density frozen-in or -out before the entropy release, namely at temperatures  $T_i > T_{NA}$ , gets maximally depleted by  $D$ .

The quantity  $D$  also allows us to quantify the critical value  $V_{PQ}^{(c)}$ , defined as the point where the three lines in the left panel of Fig. 2 intersect. Its value is obtained by imposing  $D = 1$

$$V_{PQ}^{(c)} = \left( \frac{q_\mu \sqrt{\mathcal{D}} \mu^2 M_{Pl}^2}{4\sqrt{3\pi} m_s} \right)^{\frac{1}{3}} \simeq 10^{13} \text{ GeV } q_\mu^{\frac{1}{3}} \left(\frac{\mathcal{D}}{4}\right)^{\frac{1}{6}} \left(\frac{\mu}{1 \text{ TeV}}\right)^{\frac{2}{3}} \left(\frac{1 \text{ TeV}}{m_s}\right)^{\frac{1}{3}}. \quad (2.10)$$

## 2.2 Low reheat temperature after inflation: $T_R \lesssim 10^{10}$ GeV

So far we have assumed that saxion oscillations begin during a radiation dominated era. However, this need not be the case as we do not know the temperature of reheating after inflation, which is set by the decay width of the inflaton. We now extend our analysis to low  $T_R$ .

During inflationary reheating, the temperature dependence of the Hubble parameter is different than during a radiation dominated era. An approximate solution to the coupled Boltzmann equations describing the evolution of inflaton and radiation energy densities, at early times before the inflaton decays, gives the expression for the Hubble parameter [17, 18]

$$H(T) = \frac{\sqrt{5}\pi}{6\sqrt{2}} \frac{g_*(T)}{g_*(T_R)^{1/2}} \frac{T^4}{M_{Pl} T_R^2}, \quad T > T_R. \quad (2.11)$$

Oscillations for the saxion condensate begin at  $T'_{\text{osc}}$ , when  $3H = m_s$ . We assume that  $T'_{\text{osc}}$  is less than the maximum temperature reached during this reheating era, so that  $H$  is now given by Eq. (2.11), giving

$$\begin{aligned} T'_{\text{osc}} &= \left( \frac{8 g_*(T_R)}{5 \pi^2 g_*(T'_{\text{osc}})^2} \right)^{\frac{1}{8}} (m_s M_{Pl} T_R^2)^{\frac{1}{4}} \\ &= 10^{10} \text{ GeV } \left( \frac{g_*(T_R)}{228.75} \right)^{\frac{1}{8}} \left( \frac{228.75}{g_*(T'_{\text{osc}})} \right)^{\frac{1}{4}} \left( \frac{m_s}{1 \text{ TeV}} \right)^{\frac{1}{4}} \left( \frac{T_R}{10^{10} \text{ GeV}} \right)^{\frac{1}{2}}. \end{aligned} \quad (2.12)$$

This equation makes sense only if  $T'_{\text{osc}} > T_R$ , and this condition is satisfied as long as  $T_R < T_{\text{osc}} \simeq 10^{10}$  GeV, namely the oscillation temperature given in Eq. (2.2).

The saxion oscillations for  $T < T'_{\text{osc}}$  still red-shift as non-relativistic matter, and once the inflaton finally decays the energy density stored in them results in

$$\rho_s(T_R) = m_s^2 s_I^2 \left( \frac{g_*(T_R)}{g_*(T'_{\text{osc}})} \right)^2 \left( \frac{T_R}{T'_{\text{osc}}} \right)^8. \quad (2.13)$$

Afterwards, we have the conventional thermal history described above. The only difference is the initial condition for the saxion energy density as in Eq. (2.13). This in turn gives a different expression for  $T_M$ , which is now found by imposing the condition

$$\rho_s(T_M) = \rho_s(T_R) \frac{g_*(T_M) T_M^3}{g_*(T_R) T_R^3} = \rho_R(T_M) = \frac{\pi^2}{30} g_*(T_M) T_M^4. \quad (2.14)$$

The solution of this equation simply gives

$$T'_M = \frac{30}{\pi^2} \frac{g_*(T_R)}{g_*(T'_{\text{osc}})^2} \frac{m_s^2 s_I^2 T_R^5}{(T'_{\text{osc}})^8} = \frac{75}{4} \left( \frac{s_I}{M_{\text{Pl}}} \right)^2 T_R, \quad (2.15)$$

where in the last step we have used the expression in Eq. (2.12). This expression breaks down when  $T'_M$  becomes larger than  $T_R$ , which happens if  $s_I \geq M_{\text{Pl}}/\sqrt{3}$ . We avoid this situation because the saxion condensate dominates the energy density before it starts to oscillate and consequently the Universe enters inflation.

The expression for  $T_{Rs}$  is of course unchanged, and still given by Eq. (2.6). However, the temperature for the transition to the non-adiabatic phase is changed

$$\begin{aligned} T'_{NA} &= (T'_M T_{Rs}^4)^{\frac{1}{5}} \simeq 2.5 \times 10^4 \text{ GeV} \left( \frac{T_R s_I^2}{m_s^2 V_{PQ}^4} \right)^{\frac{1}{5}} \\ &\simeq 632 \text{ GeV} \left( \frac{T_R}{10^{10} \text{ GeV}} \right)^{\frac{1}{5}} \left( \frac{s_I}{10^{16} \text{ GeV}} \right)^{\frac{2}{5}} \left( \frac{1 \text{ TeV}}{m_s} \right)^{\frac{2}{5}} \left( \frac{10^{11} \text{ GeV}}{V_{PQ}} \right)^{\frac{4}{5}}. \end{aligned} \quad (2.16)$$

Moreover, also the expression for the dilution factor changes

$$D'(T_i) = \begin{cases} 4 \times 10^5 \left( \frac{s_I}{10^{16} \text{ GeV}} \right)^2 \left( \frac{T_R}{10^{10} \text{ GeV}} \right) \left( \frac{1 \text{ TeV}}{\mu} \right)^2 \left( \frac{m_s}{1 \text{ TeV}} \right)^{\frac{1}{2}} \left( \frac{V_{PQ}}{10^{11} \text{ GeV}} \right) & T_i \geq T'_{NA} \\ 10^5 q_\mu^{-5} \left( \frac{T_i}{1 \text{ TeV}} \right)^5 \left( \frac{4}{D} \right)^{\frac{5}{2}} \left( \frac{1 \text{ TeV}}{\mu} \right)^{\frac{15}{2}} \left( \frac{m_s}{\mu} \right)^{\frac{5}{2}} \left( \frac{V_{PQ}}{10^{11} \text{ GeV}} \right)^5 & T'_{NA} \geq T_i \geq T_{Rs}. \end{cases} \quad (2.17)$$

We observe the remarkable fact that the dilution factor is proportional to  $T_R$  when  $T_i \geq T'_{NA}$ .

### 2.3 Field equations

The analytical expressions for the characteristic temperatures and the dilution factor are very useful for an order of magnitude estimate of the effect. However, they are not suited for precision

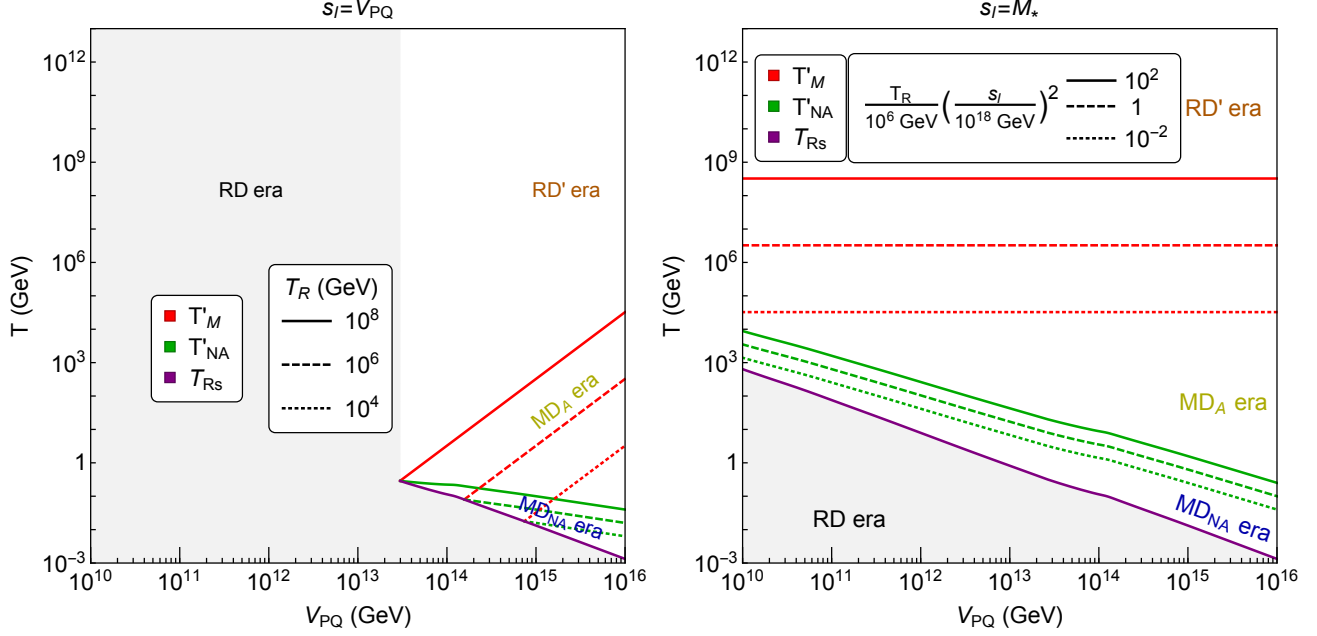


Figure 3: Cosmological eras for  $T_R \leq 10^{10}$  GeV.  $T'_M$ ,  $T'_{NA}$  and  $T_{Rs}$  as functions of  $V_{PQ}$  with  $s_I = V_{PQ}$  ( $M_*$ ) in the left (right) panel,  $\mu = m_s = 1$  TeV,  $q_\mu = 1$ , and  $\mathcal{D} = 4$ . The RD', MD<sub>A</sub>, MD<sub>NA</sub>, RD eras are labeled similar to Fig. 2, whereas some of the shadings are removed for clarity. In the right panel, both  $T_R$  and  $s_I$  are needed to specify  $T'_M$ .

calculation of relic densities. In this work we solve numerically the Boltzmann equation system describing the evolution of the saxion condensate coupled to the radiation bath.

We begin with the case where the saxion starts to oscillate after inflationary reheating, presented in Sec. 2.1. The energy density of the saxion condensate, after the onset of oscillations at  $T_{\text{osc}}$  of Eq. (2.2) or at  $T'_{\text{osc}}$  of Eq. (2.12), evolves according to

$$\frac{d\rho_s}{dt} + 3H\rho_s = -\Gamma_s\rho_s. \quad (2.18)$$

The redshift due to the Hubble expansion is accompanied by the term proportional to the saxion total decay width.

The radiation bath temperature evolves according to

$$\frac{\pi^2}{30}g_*(T) \left(1 + \frac{1}{3} \frac{d \ln g_*}{d \ln T}\right) \frac{dT^4}{dt} + 4H \frac{\pi^2}{30}g_*(T)T^4 = \Gamma_s\rho_s. \quad (2.19)$$

where  $g_*$  is the effective number of degrees of freedom contributing to the entropy density. In the limiting case where  $g_*$  is a constant, the equation takes a more familiar form

$$\frac{d\rho_{\text{rad}}}{dt} + 4H\rho_{\text{rad}} = \Gamma_s\rho_s, \quad (2.20)$$

where the radiation energy density results in

$$\rho_{\text{rad}} = \frac{\pi^2}{30} g_*(T) T^4. \quad (2.21)$$

This approximation is certainly valid at very high temperature, where the full spectrum is relativistic. At lower temperature the approximation breaks down and the error one makes by using Eq. (2.21) is at most of few percent. In our work we use Eq. (2.19), and  $g_*(T)$  is computed using the masses of the SM particles and of the SUSY particles, assumed degenerate at 1 TeV.

Finally, the time-temperature relation can be found by solving the Friedmann equation

$$H = \frac{1}{\sqrt{3} M_{Pl}} \sqrt{\rho_s + \frac{\pi^2}{30} g_*(T) T^4}. \quad (2.22)$$

The initial condition for this case is set at some high temperature  $T_0$  by

$$\rho_{Mi} = \frac{\pi^2}{30} g_*(T_M) T_M T_0^3, \quad (2.23)$$

where  $T_M$  is defined in Eq. (2.4) and our numerical studies are completely insensitive to  $T_0$ .

For the case where the saxion starts to oscillate during inflationary reheating, the numerical setup needs to be extended as follows. Firstly, we cannot ignore the inflaton anymore and we couple Eqs. (2.18) and (2.19) to the one describing the evolution of the inflaton energy density  $\rho_I$ , which takes the same form as Eq. (2.18) with the modifications  $\rho_s \rightarrow \rho_I$  and  $\Gamma_s \rightarrow \Gamma_I$ . Furthermore, we need to add the inflaton decay contribution  $\Gamma_I \rho_I$  to the right-hand side of Eq. (2.19), and the inflaton energy density on the right-hand side of Eq. (2.22). Secondly, we set the initial conditions for the saxion oscillation at the time  $3H(t_{\text{osc}}) = m_s$ , with  $H$  in this case dominated by the inflaton energy density. Since inflationary reheating is in an MD era, we can identify  $3H(t_{\text{osc}}) = 2/t_{\text{osc}}$ , and thus the initial condition  $\rho_s(t_{\text{osc}}) = m_s^2 s_I^2$  is set at the time  $t_{\text{osc}} = 2/m_s$ .

### 3 Axino and Gravitino Production

In this Section we quantify axino and gravitino production by accounting for the saxion condensate effects. We consider three different mechanisms: axino production from freeze-in, axino UV production (present only in DFSZ<sub>+</sub> theories) and gravitino UV production. For each case, we show results for the comoving number density as a function of  $V_{\text{PQ}}$ , and we consider both  $s_I = V_{\text{PQ}}$  and  $s_I = M_*$ . The results presented here are completely general and independent on where the axino and gravitino sit in the superpartner spectrum. We apply the framework to two specific spectra corresponding to High Scale and Low Scale mediation in Secs. 4.1 and 4.2 respectively.

### 3.1 Freeze-In Production of Axinos

The freeze-in production of axinos is controlled by neutralino and chargino decays and inverse decays,  $\tilde{\chi} \rightarrow \tilde{a}$ . Explicit decay widths relevant for this case are given in App. B. The evolution of the axino number density  $n_{\tilde{a}}$  is governed by the Boltzmann equation

$$\dot{n}_{\tilde{a}} + 3Hn_{\tilde{a}} = \mathcal{C}_{\text{FI}} . \quad (3.1)$$

Our goal here is to provide the expression for the collision operators  $\mathcal{C}_{\text{FI}}$ .

For a light axino, lighter than all the MSSM superpartners, freeze-in comes from neutralinos and charginos decays to axinos

$$\tilde{N}_i \rightarrow \tilde{a}h, \tilde{a}Z , \quad (3.2)$$

$$\tilde{C}_i^{\pm} \rightarrow \tilde{a}W^{\pm} . \quad (3.3)$$

The partial widths for these channels are given in Eqs. (B.14) and (B.16), respectively. On the contrary, for a heavy axino, heavier than all the neutralinos and charginos, freeze-in production is dominated by the inverse decays

$$\tilde{N}_i h, \tilde{N}_i Z \rightarrow \tilde{a} , \quad (3.4)$$

$$\tilde{C}_i^{\pm} W^{\mp} \rightarrow \tilde{a} . \quad (3.5)$$

We use the detailed-balance principle to write the collision operator in the Boltzmann equation by using the inverse reaction, namely the axino decay, with partial decay widths given in Eqs. (B.15) and (B.17). In the intermediate case, with the axino mass within the neutralinos and charginos masses, we have both types of reactions, but only the ones allowed by kinematics.

The freeze-in collision operator is a sum of the possible sources

$$\mathcal{C}_{\text{FI}} = \mathcal{C}_{\text{FI}}^{\text{n-decay}} + \mathcal{C}_{\text{FI}}^{\text{n-inverse}} + \mathcal{C}_{\text{FI}}^{\text{c-decay}} + \mathcal{C}_{\text{FI}}^{\text{c-inverse}} . \quad (3.6)$$

The first two terms account for the processes involving the neutralinos

$$\mathcal{C}_{\text{FI}}^{\text{n-decay}} = \frac{T^3}{\pi^2} \sum_{i=1}^4 \theta(m_{\tilde{N}_i} - m_{\tilde{a}}) \Gamma_{\tilde{N}_i \rightarrow \tilde{a}H} \left( \frac{m_{\tilde{N}_i}}{T} \right)^2 K_1[m_{\tilde{N}_i}/T] , \quad (3.7)$$

$$\mathcal{C}_{\text{FI}}^{\text{n-inverse}} = \frac{T^3}{\pi^2} \sum_{i=1}^4 \theta(m_{\tilde{a}} - m_{\tilde{N}_i}) \Gamma_{\tilde{a} \rightarrow \tilde{N}_i H} \left( \frac{m_{\tilde{a}}}{T} \right)^2 K_1[m_{\tilde{a}}/T] , \quad (3.8)$$

where  $K_1$  is the first modified Bessel function of the second kind. The Heaviside step function  $\theta$  makes sure that only the kinematically allowed channels are accounted for. The correspondent collision operators for the charginos are

$$\mathcal{C}_{\text{FI}}^{\text{c-decay}} = \frac{2T^3}{\pi^2} \sum_{i=1}^2 \theta(m_{\tilde{C}_i} - m_{\tilde{a}}) \Gamma_{\tilde{C}_i \rightarrow \tilde{a}H} \left( \frac{m_{\tilde{C}_i}}{T} \right)^2 K_1[m_{\tilde{C}_i}/T] , \quad (3.9)$$

$$\mathcal{C}_{\text{FI}}^{\text{c-inverse}} = \frac{T^3}{\pi^2} \sum_{i=1}^2 \theta(m_{\tilde{a}} - m_{\tilde{C}_i}) \Gamma_{\tilde{a} \rightarrow \tilde{C}_i H} \left( \frac{m_{\tilde{a}}}{T} \right)^2 K_1[m_{\tilde{a}}/T] . \quad (3.10)$$

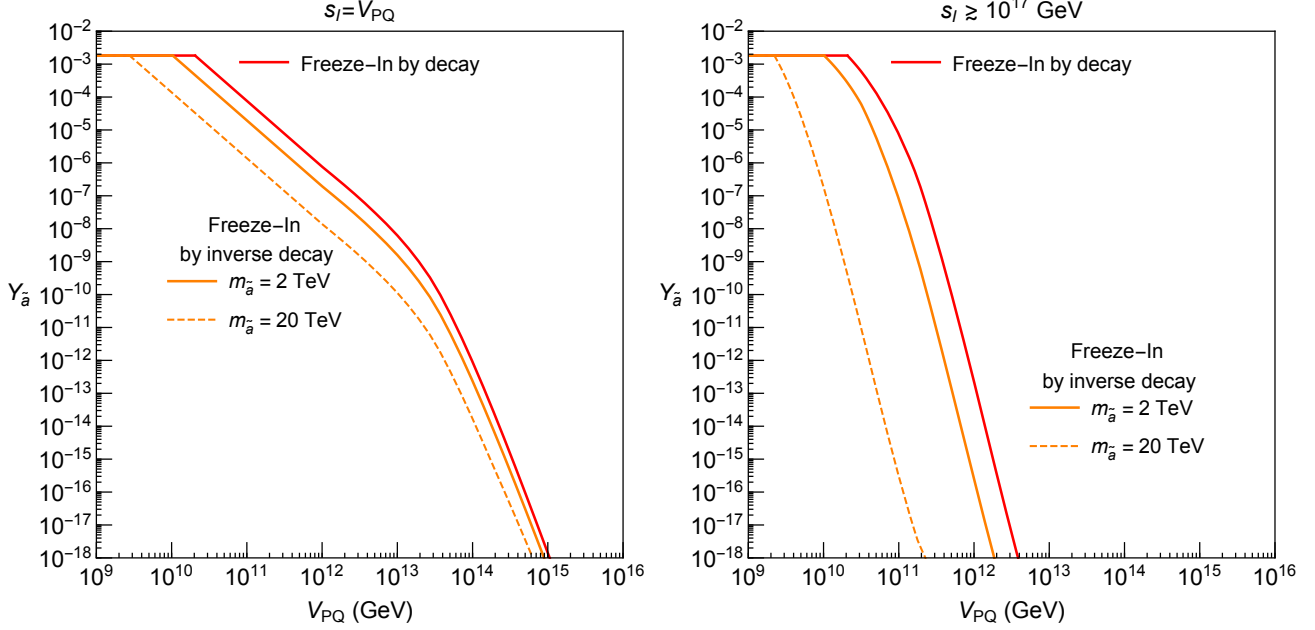


Figure 4: The axino yield from neutralino decays (red) for  $m_{\tilde{a}} \ll 1$  TeV, and neutralino inverse decays (orange) for  $m_{\tilde{a}} = 2$  and 20 TeV. In both panels,  $2M_1 = M_2 = \mu = 1$  TeV,  $m_s = 500$  GeV,  $\tan \beta = 2$ ,  $q_\mu = 2$ , and  $\mathcal{D} = 4$ ; while  $s_I = V_{PQ}$  ( $M_* \gtrsim 10^{17}$  GeV) for the left (right) panel.

The results for the axino comoving density are shown in Fig. 4, where the saxion dilution is computed using the cosmology of section 2.1 with  $T_R \gtrsim 10^{10}$  GeV. In each of the two panels, we fix the MSSM mass parameters as in the caption, and compute the axino comoving density as a function of  $V_{PQ}$ .

### 3.2 UV Production of Axinos

This gravitino problem is greatly exacerbated in PQ theories with heavy matter since then UV production of axinos also generally occurs. The combination of the two UV production mechanisms provides a particularly powerful upper bound on  $T_R$  [12]. A complication in computing the UV contribution to axino production is that if the heaviest matter carrying both PQ charges and gauge charges,  $\Phi$ , has a mass  $M_\Phi < T_R$  then the UV production is cutoff at  $M_\Phi$  [11]; thus  $Y_{\tilde{a}}^{UV}$  is model-dependent. In the DFSZ<sub>+</sub> theory we take  $M_\Phi \gtrsim T_R$ , so that the UV axino production is cutoff at  $T_R$ . The axino mass is expected to be of order the gravitino mass or larger, in which case, in DFSZ<sub>+</sub> with  $V_{PQ} \sim 10^{12}$  GeV and TeV scale supersymmetry,  $T_R \lesssim 10^6$  GeV [12]. Here we show that the limits from UV production of axinos is greatly ameliorated by the decay of the saxion condensate, with resulting limits depending on  $(V_{PQ}, m_{\tilde{a}})$ .

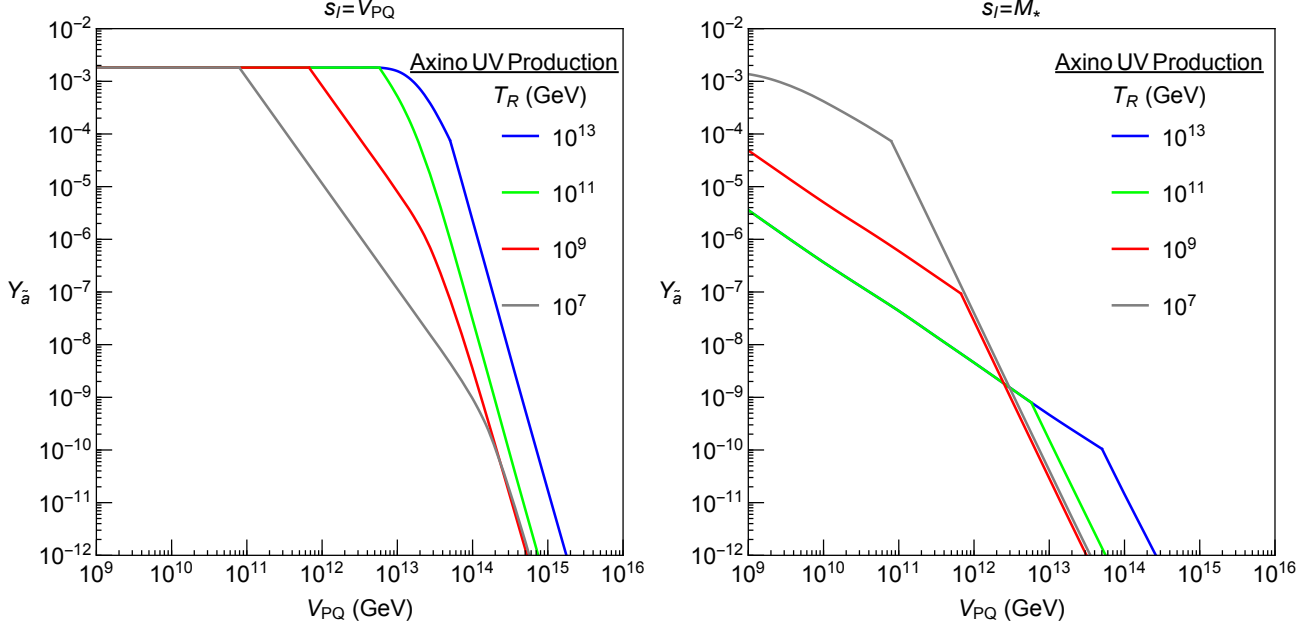


Figure 5: The axino yield from UV scattering. In both panels,  $m_s = \mu = 1$  TeV,  $q_\mu = 2$ , and  $\mathcal{D} = 4$ ; while  $s_I = V_{PQ}$  ( $M_* = 3 \times 10^{16}$  GeV) for the left (right) panel. We take the axion domain wall number  $N_{DW} = 6$  for the axion decay constant  $f_a = \sqrt{2}V_{PQ}/N_{DW}$ .

With UV production of axinos cut off at  $T_R$ , scattering leads to an axino yield [9]

$$Y_a^{UV}|_+ \sim 2 \times 10^{-6} g_3^6 \ln\left(\frac{3}{g_3}\right) \left(\frac{N_{DW}}{6}\right)^2 \left(\frac{T_R}{10^{10} \text{ GeV}}\right) \left(\frac{10^{14} \text{ GeV}}{V_{PQ}}\right)^2 \quad (3.11)$$

where  $g_3$  is the strong gauge coupling. As elsewhere, we take  $N_{DW} = 6$ . The yields of axinos and gravitinos should not exceed the thermal equilibrium value

$$Y_{eq} = \frac{135\zeta(3)g}{8\pi^4 g_*} \simeq 1.8 \times 10^{-3} \left(\frac{g}{2}\right) \left(\frac{228.75}{g_*}\right), \quad (3.12)$$

where  $\zeta$  is the zeta function and the internal degrees of freedom  $g$  is 2 (4) for the axino (gravitino).

To include the effect of saxion dilution, we divide the axino abundance by the dilution factor computed numerically. Since axino UV production occurs before the saxion injects the entropy, the dilution factor is simply the ratio of the total entropy before and after the saxion MD era.

The results for the axino abundance are shown in Fig. 5, for some values of  $T_R \gtrsim 10^{10}$  GeV that have saxion dilution of Sec. 2.1 and others of Sec. 2.2 with  $T_R \lesssim 10^{10}$  GeV. We take  $s_I = V_{PQ}$  ( $M_* = 3 \times 10^{16}$  GeV) in the left (right) panel. Note that for a sufficiently low  $V_{PQ}$ , the axino reaches thermal equilibrium, in which case we will use the equilibrium value of the yield in Eq. (3.12). In particular, the sharp kink in each of the curve is due to the transition from the thermal value  $Y_{eq}$  to the yield from UV scattering. In the left panel, the smooth change of

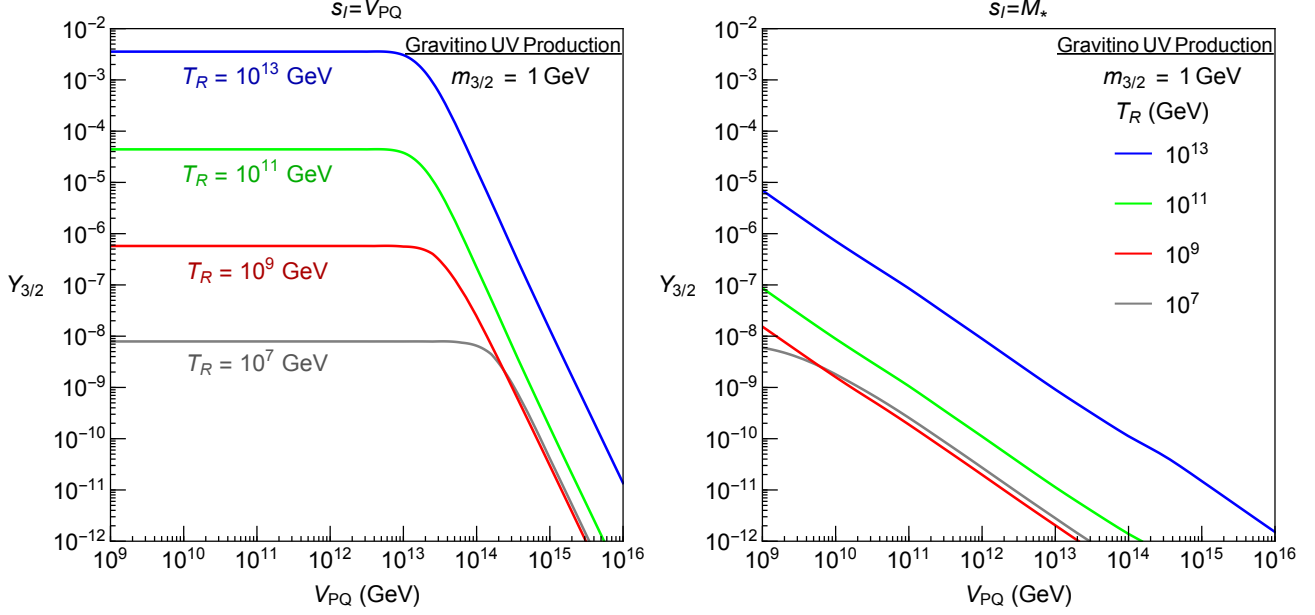


Figure 6: The gravitino yield from UV scattering and saxion dilution for  $s_I = V_{PQ}$  ( $M_* = 3 \times 10^{16}$  GeV) in the left (right) panel. In both panels,  $m_s = \mu = 1$  TeV,  $q_\mu = 2$ ,  $\mathcal{D} = 4$ , and the unified gaugino mass is 2 TeV and  $m_{3/2} = 1$  GeV. The yield scales as  $Y_{3/2} \propto 1/m_{3/2}^2$ , as long as  $Y_{3/2}$  is below its equilibrium value.

the slope at  $V_{PQ} \sim 10^{13-14}$  GeV is due to the emergence of the saxion MD era demonstrated in Figs. 2 and 3. In the right panel, the dilution effect is present for the entire range of  $V_{PQ}$ . In the case where  $T_R \lesssim 10^{10}$  GeV, one interesting feature is that the diluted abundance is (almost) independent of  $T_R$  because both dilution in Eq. (2.17) and production in Eq. (3.11) are proportional to  $T_R$  (other than the mild dependence on  $T_R$  in  $g_3$ ).

### 3.3 UV Production of Gravitinos

In supersymmetric theories UV production of gravitinos generally limits the reheat temperature after inflation,  $T_R$  [29]. The abundance of gravitinos from scattering at  $T_R$  is

$$Y_{3/2}^{UV} \sim 6 \times 10^{-12} \frac{T_R}{10^{10} \text{ GeV}} \sum_i \gamma_i(T_R) \left( 1 + \frac{m_i^2}{3m_{3/2}^2} \right), \quad (3.13)$$

where  $\gamma_i(T_R) \sim (0.02, 0.08, 0.25 - 0.4, 0.02)$  is given in Ref. [10] and  $m_i = (m_{(1,2,3)}, A_t)$  is the gaugino mass of  $(U(1), SU(2), SU(3))$  and the  $A$ -term of the top Yukawa coupling.

Similar to Sec. 3.2, we calculate the final gravitino abundance by dividing the yield by the dilution factor computed numerically.

The numerical results for the gravitino abundance are shown in Fig. 6 for  $T_R \geq 10^{10}$  GeV ( $T_R \leq 10^{10}$  GeV) with saxion dilution of Sec. 2.1 (Sec. 2.2). In the left panel, with  $s_I =$



$V_{PQ}$ , there is no dilution for  $V_{PQ} < V_{PQ}^{(c)}$  because the condensate is too small for the saxions to dominate before they decay. The key feature is the rapid dilution for  $V_{PQ} > V_{PQ}^{(c)}$ , with  $V_{PQ}^{(c)} \sim 10^{13}$  GeV for  $T_R \gtrsim 10^{10}$  GeV and growing for smaller  $T_R$ . In the right panel  $s_I = M_* = 3 \times 10^{16}$  GeV is large everywhere, so a saxion dominated MD era occurs at much lower values of  $V_{PQ}^{(c)}$ , leading to dilution at low  $V_{PQ}$ . For  $T_R < 10^{10}$  GeV, the final diluted yield is (almost) independent of  $T_R$  (other than  $\gamma_i(T_R)$  in Eq. (3.13)).

## 4 Axino and Gravitino as the Lightest Superpartners

We classify the superpartner spectra according to the size of the mediation scale for supersymmetry breaking,  $M_{\text{mess}}$ . Superpartner masses arise from the effective operators

$$\mathcal{L}_{\text{mess}} = \frac{c_a}{M_{\text{mess}}} \int d^2\theta X W_a^\alpha W_{a\alpha} + \frac{c_Q^2}{M_{\text{mess}}^2} \int d^2\theta X^\dagger X Q^\dagger Q \quad (4.1)$$

where the superfield  $X$ , defined in Eq. (A.9), has a SUSY breaking F-component. We take the model-dependent coefficients  $c_a$  and  $c_Q$  to be comparable  $c_Q \simeq c_a$ ; the spectrum is not split.

In Sec. 4.1 we consider  $M_{\text{mess}}$  of order  $M_{\text{Pl}}$ , which can be broadly identified with “gravity mediation.” The gravitino for this case cannot be much lighter than the other superpartners. This has to be contrasted with the low mediation scale case elaborated in Sec. 4.2,  $M_{\text{mess}} \ll M_{\text{Pl}}$ , where the gravitino is much lighter than other superpartners. We focus our attention on the spectra where the axino and the gravitino are both lighter than all the other superpartners. However, for gravity mediation we do not commit to any relative hierarchy between them, and consider both axino and gravitino LSP cases.

For both high and low mediation scales, axinos and gravitinos are produced in the early universe through the various mechanisms discussed in the previous Section. These processes produce both the NLSP and the LSP, and they all contribute to the present dark matter abundance, which today is made of LSP particles only. Highly relativistic axions are produced in NLSP decays, which make a negligible contribution to dark radiation. Furthermore, since the final products are the LSP and the axion, these decays are not subject to BBN limits [30–32]. As we will see in this Section, the origin of the current dark matter abundance is typically due to either NLSP or LSP production, unless we consider peculiar parameter space regions.

Before we discuss the high and low scale cases in detail, we highlight the main features of our framework.

- **Warm Dark Matter from NLSP Decays.** Dark matter from LSP production is always cold. On the contrary, dark matter from NLSP production and decay could be hot, warm or cold, depending on the ratio of NLSP and LSP masses and the NLSP decay lifetime. The LSP is a gauge singlet extremely weakly coupled to the radiation bath, and thus DM particles coming from NLSP decays just lose their momenta by pure free streaming. This has the effect of potentially washing out cosmological perturbations at small scales through free streaming, and this scenario is severely constrained by Lyman- $\alpha$  forest observations [33–35], bounding

the free streaming length to be less than  $\simeq 1$  Mpc. Interestingly, if the free streaming length is consistent with large scale structure and not too small it can address some large scale structure (LSS) issues that are indicated by simulations of collisionless cold dark matter [36]. Baryonic feedback effects can explain some discrepancies [37, 38], although there is much debate on this [39, 40].

If the axino is the NLSP, it decays to longitudinal gravitinos (i.e. goldstino) via the effective operators given in Eq. (B.22), giving a lifetime from Eq. (B.25) of

$$\tau_{\tilde{a}} = \Gamma_{\tilde{a} \rightarrow a \psi}^{-1} \simeq 1.2 \times 10^4 \text{ sec} \left( \frac{m_{3/2}}{100 \text{ GeV}} \right)^2 \left( \frac{1 \text{ TeV}}{m_{\tilde{a}}} \right)^5. \quad (4.2)$$

The associated free streaming length for free streaming gravitinos is approximately given by the expression in Eq. (C.8), which for the lifetime above reads

$$\lambda_{\text{FS}}^{\psi} \simeq 0.6 \text{ Mpc} \left( \frac{1 \text{ TeV}}{m_{\tilde{a}}} \right)^{3/2} \left[ 1 + 0.15 \log \left( \frac{m_{\tilde{a}}}{1 \text{ TeV}} \right) \right]. \quad (4.3)$$

This expression holds as long as  $m_{\tilde{a}} \gg m_{3/2}$ . Remarkably, the gravitino free streaming length depends only on the axino mass, and for TeV scale axinos is not in conflict with Lyman- $\alpha$  forest observations and in the correct ballpark to address LSS anomalies. Numerical results are shown in the left panel of Fig. 7, where we draw  $\lambda_{\text{FS}}$  isocontours in the  $(m_{\tilde{a}}, m_{3/2})$  plane. These results are derived by using the full derivation of  $\lambda_{\text{FS}}$  in App. C. In the  $m_{\tilde{a}} \gg m_{3/2}$  regime, where the free streaming length is approximated by Eq. (4.3), the isocontours are vertical lines in the  $(m_{\tilde{a}}, m_{3/2})$  plane.

For gravitino NLSP, the decays to axinos are mediated by the operator in Eq. (B.18). We assume that the decay to saxion and axino final state is kinematically forbidden, thus the decay width is half of the expression in Eq. (B.20), to account for decays to axion and axino only. The resulting lifetime is

$$\tau_{3/2} = \Gamma_{\psi \rightarrow a \tilde{a}}^{-1} \simeq 8.5 \times 10^6 \text{ sec} \left( \frac{1 \text{ TeV}}{m_{3/2}} \right)^3. \quad (4.4)$$

To simplify the discussion we take the axino mass to be of order 1 TeV – i.e. not far below the other superpartner masses. Thus, while Eq. (4.2) can be used for both High and Low Scale mediation, Eq. (4.4) is used only in High Scale mediation. In both equations we have ignored phase space factors that become relevant when the NLSP and LSP masses are comparable. The axino free streaming length, in the limit where  $m_{\tilde{a}} \ll m_{3/2}$ , is approximately given by

$$\lambda_{\text{FS}}^{\tilde{a}} \simeq 1.2 \text{ Mpc} \left( \frac{2 \text{ TeV}}{m_{3/2}} \right)^{1/2} \left( \frac{1 \text{ TeV}}{m_{\tilde{a}}} \right) \left[ 1 + 0.1 \log \left( \left( \frac{m_{3/2}}{2 \text{ TeV}} \right)^{1/2} \left( \frac{m_{\tilde{a}}}{1 \text{ TeV}} \right) \right) \right]. \quad (4.5)$$

The full result is shown in the right panel of Fig. 7. In the  $m_{\tilde{a}} \ll m_{3/2}$  region, the free streaming isocontours are along the lines  $m_{3/2} m_{\tilde{a}}^2 = \text{const}$ , consistently with the approximate

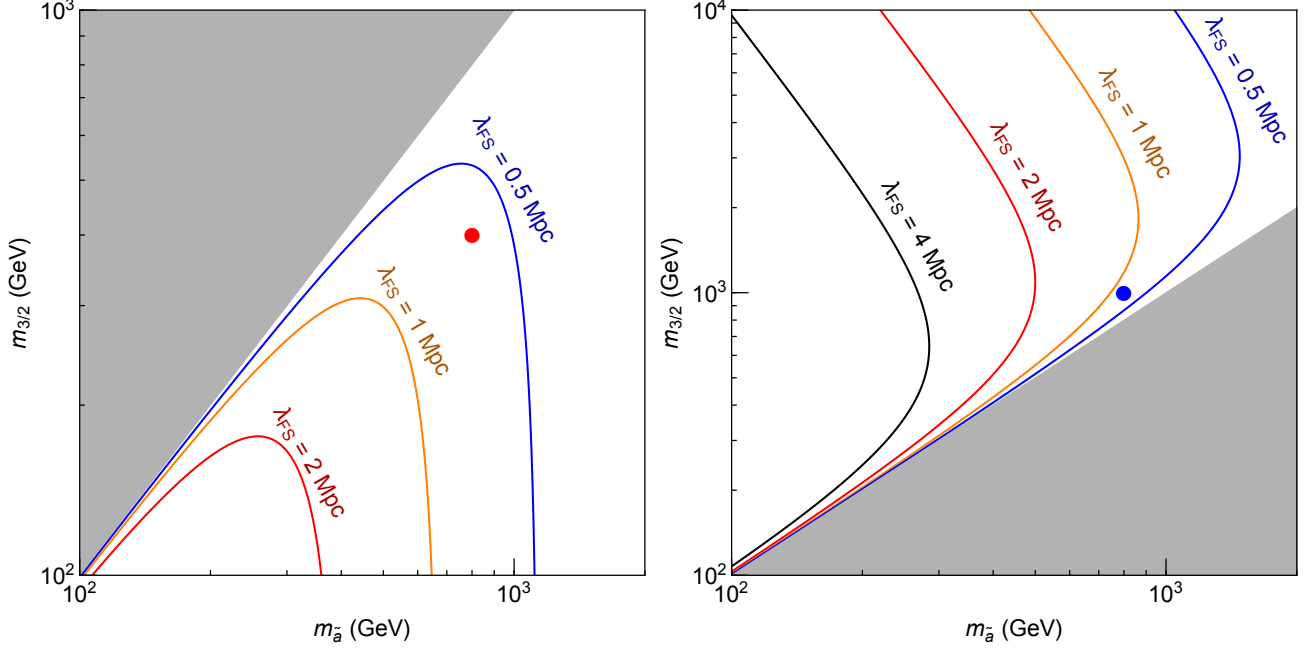


Figure 7: Free streaming length  $\lambda_{FS}$  for the warm dark matter component. In the left (right) panel we show the result for gravitino (axino) LSP produced through the NLSP axino (gravitino) decay process  $\tilde{a} \rightarrow \psi a$  ( $\psi \rightarrow \tilde{a} a$ ). The red and blue dots label the spectra we choose for High Scale mediation in Sec. 4.1. For Low Scale mediation in Sec. 4.2, we only need to require  $m_{\tilde{a}} \gtrsim 650$  GeV since the free streaming length becomes independent of  $m_{3/2}$ .

expression in Eq. (4.5). Lyman- $\alpha$  bounds are evaded for sufficiently heavy gravitino and/or axino, and issues with LSS can be addressed again by TeV scale superpartners.

A related noteworthy example is the case of gravitinos coming from LOSP freeze-out and decays [41, 42], which in our case is made irrelevant by the saxion condensate dilution.

- **Displaced Signals at Colliders.** If the lightest observable-sector supersymmetric partner (LOSP) is a neutralino  $\tilde{N}_1$ , its decay to the axino and Higgs/longitudinal Z bosons will leave missing energy and a displaced vertex. The decay length for this channel can be obtained from the associated decay width given in Eq. (B.14) of App. B,

$$c\tau_{\tilde{N}_1 \rightarrow \tilde{a}} \simeq 2.5 \text{ m} \frac{1}{k_{\tilde{a}}} \left( \frac{2}{q_\mu} \right)^2 \left( \frac{\mu}{m_{\tilde{N}_1}} \right) \left( \frac{10^3 \text{ GeV}}{\mu} \right)^3 \left( \frac{V_{PQ}}{10^{12} \text{ GeV}} \right)^2. \quad (4.6)$$

Here, we define the mixing factor  $k_{\tilde{a}} \equiv |s_\beta R_{31}|^2 + |c_\beta R_{41}|^2$ , with  $R_{ij}$  the neutralino mixing matrix (for details see Eqs. (B.10) and (B.14)). In the pure Higgsino LOSP limit, with decoupled bino and wino,  $k_{\tilde{a}}$  becomes 1/2 and is thus independent of  $\beta$ . On the other hand,  $k_{\tilde{a}}$  will be suppressed when the LOSP is bino- or wino-like.

For Low Scale mediation with  $m_{3/2} \lesssim 1$  MeV, the decay channel of neutralinos to gravitinos becomes sufficiently enhanced to dominate over the axino final state, giving a decay length

$$c\tau_{\tilde{N}_1 \rightarrow \tilde{G}} \simeq 2 \text{ m} \frac{1}{k_{\tilde{G}}} \left( \frac{1 \text{ TeV}}{m_{\tilde{N}_1}} \right)^5 \left( \frac{m_{3/2}}{100 \text{ keV}} \right)^2, \quad (4.7)$$

where  $k_{\tilde{G}}$  contains the analogous mixing factors given in the decay widths Eqs. (B.26)–(B.29).

In the following sub-sections, we show the LOSP decay length using the total decay rate including axino and gravitino in the final states. To obtain  $\Gamma_{\tilde{N}_1 \rightarrow \tilde{a}}$ , we use the values of  $V_{PQ}$  determined from the observed dark matter abundance. As discussed in Sec. 2, the amount of saxion dilution depends on the value of  $V_{PQ}$ . Therefore, even though gravitino UV production rate is independent of  $V_{PQ}$ , the saxion dilution needed for the overproduction fixes  $V_{PQ}$  when other parameters are specified. For the axino UV and FI mechanisms, the production rate also depends on  $V_{PQ}$  and thus makes a more correlated prediction of  $V_{PQ}$  along with saxion dilution. On the other hand,  $\Gamma_{\tilde{N}_1 \rightarrow \tilde{G}}$  can be calculated once the gravitino mass is chosen and again this decay channel only becomes relevant for very low  $m_{3/2}$ .

The lifetime that can be probed at the LHC and future colliders depends on the total production cross section of supersymmetric particles, which we quote for the case of degenerate squark and gluino masses,  $\tilde{m}$  [43]. For  $\tilde{m} = (1.5, 2.5)$  TeV, at  $\sqrt{s} = 14$  TeV this cross section is of order (100, 1) fb, so that planned runs of the LHC will allow ATLAS and CMS to reach  $c\tau$  of order (100, 10)m. Recently, a surface detector called MATHUSLA [44] has been proposed to search for (ultra) long-lived particles at the LHC and future colliders. At the LHC, with  $30 \text{ ab}^{-1}$  at  $\sqrt{s} = 14$  TeV, a low background environment allows a reach in  $c\tau$  of order  $(10^5, 10^3)$ m for  $\tilde{m} = (1.5, 2.5)$  TeV. At a future 100 TeV collider [45], MATHUSLA or a forward detector [44] can be sensitive to  $c\tau$  of order  $(10^7, 10^5)$  m for  $\tilde{m} = (3, 8)$  TeV, giving a susy production cross section of  $(10^3, 10)$  fb.

- **Axion Dark Radiation.** Saxions can decay to axions with a rate given by Eq. (B.2) if  $\kappa$  does not vanish due to symmetry. Using the branching ratio of the saxion to the visible sector and to axions, we predict the amount of dark radiation to be [20]

$$\Delta N_{eff} = 3 \frac{\rho_a}{\rho_\nu} \simeq \frac{43}{112} \left( \frac{4}{\mathcal{D}} \right) \left( \frac{g_*(1 \text{ MeV})}{10.75} \right) \left( \frac{\kappa}{q_\mu} \right)^2 \left( \frac{m_s}{\mu} \right)^4. \quad (4.8)$$

The Planck experimental bound [46] is  $\Delta N_{eff} < 0.6$ . The proposed CMB Stage-IV experiment [47] can be sensitive to  $\Delta N_{eff} = 0.03$ .

## 4.1 High Scale or “Gravity” Mediation

### 4.1.1 The DFSZ<sub>0</sub> Theory

In the the DFSZ<sub>0</sub> theory, the axino is dominantly produced by IR freeze-in, as discussed in Sec. 3.1. Since the axino is lighter than the superpartners in the thermal bath, FI occurs via

## High Scale mediation: DFSZ<sub>0</sub>

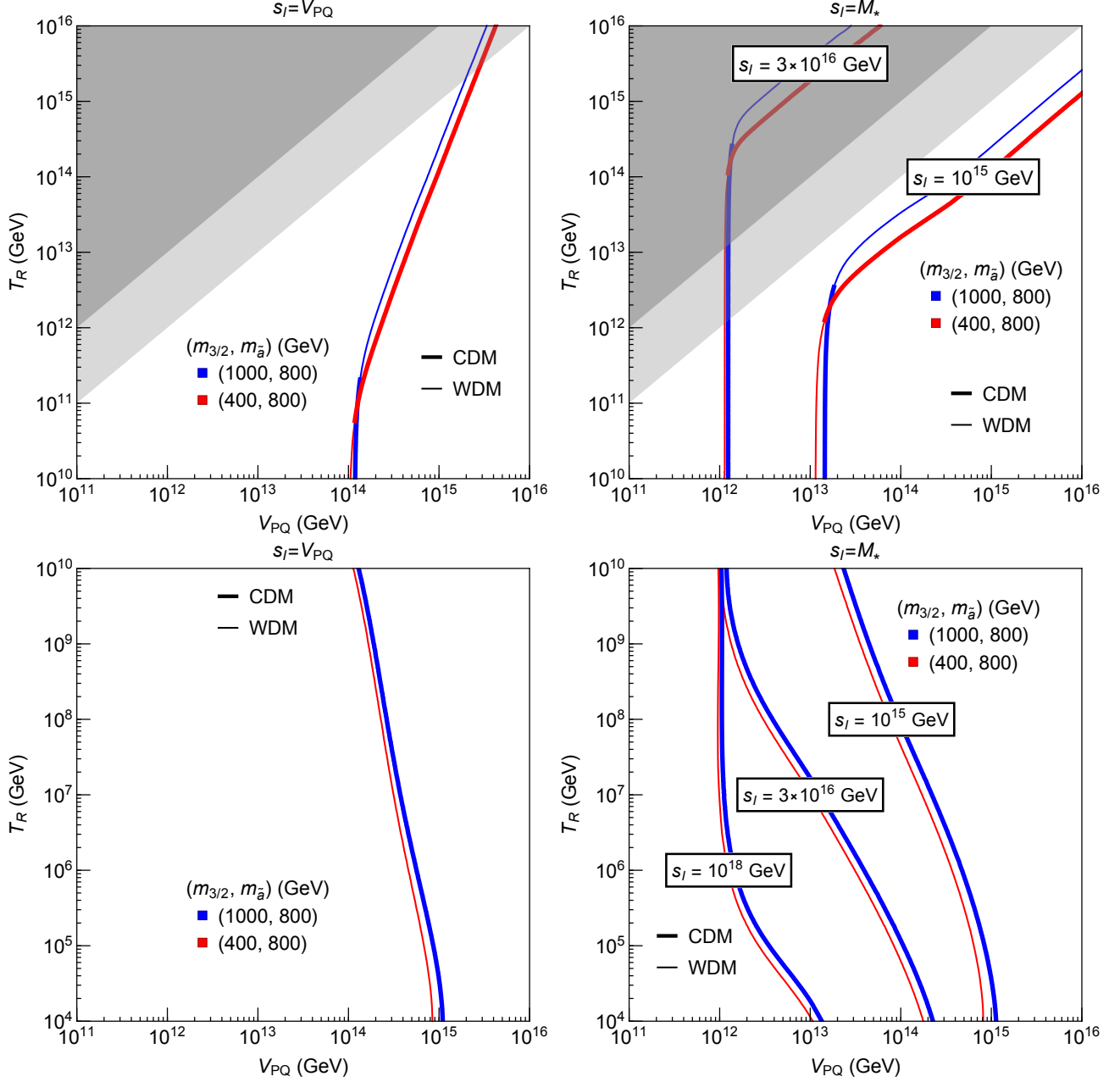


Figure 8: Contours of  $\Omega h^2 = 0.11$  from Axino freeze-in and Gravitino UV production. We fix  $q_\mu = 2$ ,  $\mathcal{D} = 4$ ,  $\tan \beta = 2$ , and  $M_2/2 = M_1 = \mu = 1$  TeV and  $m_s = 300$  GeV. The top (bottom) row is for the cosmology with  $T_R \gtrsim (\lesssim) 10^{10}$  GeV discussed in Sec. 2.1 (Sec. 2.2).

## High Scale mediation: DFSZ<sub>0</sub> + Neutralino LOSP

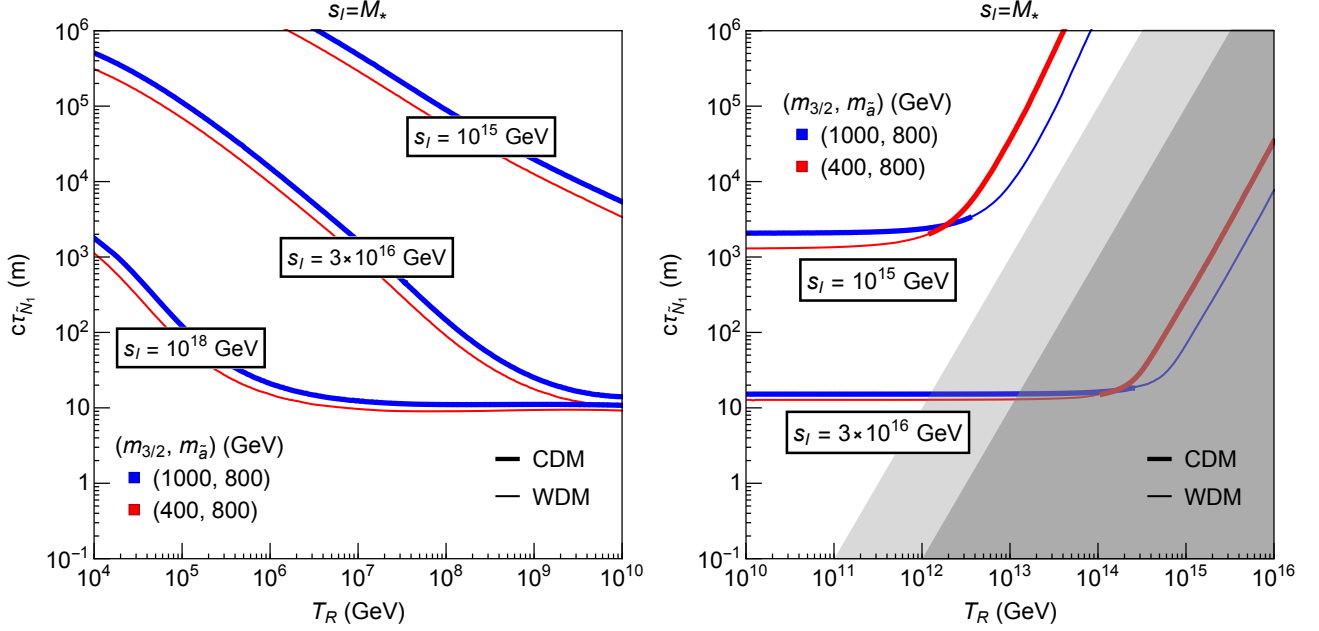


Figure 9: The decay length of the neutralino LOSP to the axino and the Higgs/Z boson, predicted by determining  $V_{PQ}$  from  $\Omega h^2 = 0.11$  using Fig. 8. We fix  $q_\mu = 2$ ,  $\mathcal{D} = 4$ ,  $\tan \beta = 2$ , and  $M_2/2 = M_1 = \mu = 1$  TeV and  $m_s = 300$  GeV. The left (right) panel is for the cosmology with  $T_R \lesssim (\gtrsim) 10^{10}$  GeV discussed in Sec. 2.2 (Sec. 2.1).

decays of neutralinos and charginos with rates proportional to  $1/V_{PQ}^2$  given by Eqs. (3.7) and (3.9). On the other hand, gravitinos are populated by the UV scattering of quarks, gluons, and their superpartners with an abundance given by Eq. (3.13), which is proportional to  $T_R$ . Both production sources are heavily diluted by the decay of the saxion condensate, which also makes the LOSP freeze-out and decay contribution negligible.

We compute the total DM abundance from these LSP and NLSP production sources in terms of  $V_{PQ}$  and  $T_R$  and draw contours of  $\Omega h^2 = 0.11$  in the  $(V_{PQ}, T_R)$  plane in Fig. 8. After decaying to the LSP, the NLSP number density is transferred to that of the LSP, and therefore we only need the LSP mass to compute the final DM abundance. In the left two panels, we take  $s_I = V_{PQ}$ , and in the right two panels we take  $s_I = M_*$  and give contours for  $M_* = (10^{15}, 3 \times 10^{16}, 10^{18})$  GeV. The top two panels have  $T_R > 10^{10}$  GeV and are therefore described by the cosmology in Sec. 2.1, while the bottom two panels have  $T_R < 10^{10}$  GeV and are described by the cosmology in Sec. 2.2.

In the upper two panels, for each value of  $s_I$  two contours are shown, the blue one is an example of an axino LSP while the red one is an example of gravitino LSP. The vertical parts of the contours have axino FI as the dominant production mechanism and hence are independent

of  $T_R$ , while the parts of the contour with positive constant slope have UV gravitino production dominate. When freeze-in occurs above  $T_{NA}$ , the dilution factor from the saxion condensate is proportional to  $s_I^2 V_{PQ}$ , which is much larger in the right panel than in the left panel. This means that the production needs to be much larger in the right panel than the left, and hence the contours in the right panel are at much lower  $V_{PQ}$ . This also explains why in the right panel, as  $s_I$  is increased from  $10^{15}$  GeV to  $10^{16}$  GeV, the contours move to lower  $V_{PQ}$ . However, for  $s_I > 10^{16}$  GeV a new regime is entered where freeze-in occurs during the  $MD_{NA}$  era and dilution becomes independent of  $T_M$  and therefore of  $s_I$ . Hence, the vertical contours for  $s_I = 3 \times 10^{16}$  GeV and  $10^{18}$  GeV differ slightly only because of a different  $m_{LSP}$ .

When UV gravitino production dominates, the difference in the slopes of the contours results from the dilution factor, scaling as  $V_{PQ}^3$  in the left panel and  $V_{PQ}$  in the right panel. At large  $T_R$  where UV gravitino production dominates the blue contours are well above the red ones; this is because  $Y_{3/2} \propto 1/m_{3/2}^2$  and the blue contours have larger  $m_{3/2}$  and hence need larger  $T_R$  to compensate. On the other hand, at lower  $T_R$  where axino FI dominates,  $Y_{\tilde{a}}$  is independent of  $m_{\tilde{a}}$  and  $m_{3/2}$ , so that the red and blue  $\Omega h^2$  contours differ only because of  $m_{LSP}$ .

Each contour is divided into thick and thin parts. The thick parts indicate cold dark matter (CDM) where NLSP production is sub-dominant. The thin parts label the warm dark matter (WDM) case where the component of dark matter from the NLSP decay constitutes more than 50% of the total abundance. The thin lines may be relevant for understanding possible difficulties with pure CDM, as in core-cusp, too big to fail and missing satellite problems.

A key point emerges from comparing the contours in the two upper panels of Fig. 8 with the contour for High Scale mediation ( $m_{3/2} = 100$  GeV) in Fig. 1, where the saxion condensate is absent. *The saxion condensate increases the maximum value of  $T_R$  from  $10^8$  GeV to  $10^{16}$  GeV.* This allows very high reheat temperatures after inflation<sup>4</sup>, so that baryogenesis may occur at very high temperatures. The upper bound on  $T_R$  now arises because inflation only gives a saxion condensate if PQ symmetry is broken before inflation. The precise constraint on  $T_R$  is dependent on the model for the PQ phase transition and on the model for reheating after inflation. For instantaneous reheating we expect the condition to typically be  $T_R < V_{PQ}$  corresponding to the unshaded region of Fig. 8. However, certain theories may have PQ breaking before inflation even for  $T_R$  somewhat higher than  $V_{PQ}$ , so that for these theories the lightly shaded region also becomes physical. We expect the dark shaded region to be unphysical in all models. On the other hand, if the inflaton decay rate is slow,  $T_R$  could be much below the energy scale of inflation, lowering the shaded bands and reducing the maximal allowed value of  $T_R$ . A reduction by a few orders of magnitude would still allow  $T_R$  to be sufficiently large for leptogenesis.

Another key point emerges from comparing the contours in the two upper panels of Fig. 8 with the contour for High Scale mediation ( $m_{3/2} = 100$  GeV) in Fig. 1. *For large  $s_I = M_*$ , the saxion condensate lowers the minimal value of  $V_{PQ}$  by several orders of magnitude.* An important part of the axino problem is that the minimal value of  $V_{PQ}$  is so large –  $4 \times 10^{14}$  GeV

---

<sup>4</sup>The largest possible values of  $T_R$  and  $V_{PQ}$ , of order  $(10^{15} - 10^{16})$  GeV, are excluded by isocurvature density perturbations if there is a sufficient contribution of misalignment axions to dark matter. In our figures we do not show any such excluded region, as the bound from such perturbations can be avoided if the axion misalignment angle  $\theta_{mis}$  is sufficiently small and/or  $N_{DW}$  is sufficiently large.



for  $m_{3/2} = 100$  GeV – that misalignment axions overclose the universe unless the misalignment angle is very small. This difficulty is removed with a saxion condensate because the decay of the condensate also dilutes misalignment axions, so that they typically give sub-dominant contributions to dark matter for  $f_a \lesssim 10^{15}$  GeV and misalignment angles order unity [13, 20]. Since  $V_{PQ}$  is larger than  $f_a$  by  $N_{DW}/\sqrt{2}$ , which is often an order of magnitude, axions are typically sub-dominant on all the contours of Fig. 8, although they could give a comparable contribution when  $V_{PQ}$  is of order  $(10^{15} - 10^{16})$  GeV.

In the lower two panels, for  $s_I = 10^{15}$  GeV and  $3 \times 10^{16}$  GeV, freeze-in occurs above  $T'_{NA}$ , so that the dilution factor is proportional to  $T_R$ , as seen in Eq. (2.15), and the axino FI abundance depends on  $T_R$ . In particular, a decrease in  $T_R$  is compensated by an increase in  $V_{PQ}$  at a rate that depends on the cosmological era during FI. However, for  $s_I = 10^{18}$  GeV much of the contour is still vertical as freeze-in occurs during  $MD_{NA}$ . For very high  $s_I$  there is a very robust prediction for  $V_{PQ}$  from axino freeze-in dark matter.

If the LOSP is a neutralino, its decay length, Eq. (4.6), can be predicted by determining  $V_{PQ}$  from the dark matter abundance. The prediction shown in Fig. 9 is obtained by inverting the two axes in the right panels of Fig. 8 and converting the  $V_{PQ}$  axis to the decay length using Eq. (4.6). The left (right) panel corresponds to the cosmology of  $T_R$  less (greater) than  $10^{10}$  GeV discussed in Sec. 2.2 (Sec. 2.1). As explained for Fig. 8, for axino FI a larger saxion condensate (higher  $s_I$ ) leads to a lower  $V_{PQ}$ , which in turn gives a shorter LOSP decay length. However, this behavior does not continue for an arbitrarily high  $s_I$ : once  $s_I$  is sufficiently high, the axino freeze-in occurs during the  $MD_{NA}$  era and the abundance becomes insensitive to  $s_I$  [7]. Consequently, for  $T_R > 3 \times 10^9$  GeV and any  $s_I > 10^{16}$  GeV, there is a very robust prediction of  $c\tau_{LOSP} \simeq 10$  m. In the left panel, as  $T_R$  drops FI transitions to occurring in  $MD_A$ , so that the dilution factor also drops and  $V_{PQ}$  and  $c\tau_{LOSP}$  increase. As in Fig. 8, the thin parts of contours give warm dark matter from NLSP decay.

#### 4.1.2 The DFSZ<sub>+</sub> Theory

In addition to the axino FI and gravitino UV contributions existing in DFSZ<sub>0</sub> theories, there is also axino production from UV scattering discussed in Sec. 3.2 for DFSZ<sub>+</sub> theories. In a setting similar to Fig. 8, we show the results for the total abundance in Fig. 10 as a function of  $T_R$  and  $V_{PQ}$ . Gravitino production is everywhere sub-dominant. In fact UV axino production dominates everywhere, except for  $T_R$  less than about  $10^6$  GeV where axino freeze-in becomes important. The blue and red curves, corresponding to axino and gravitino LSP, nearly coincide; they differ only because the LSP mass differs by a factor of two between the curves.

The parametric dependence of the contours can be understood from  $\Omega h^2 \propto Y_{\tilde{a}} m_{LSP}/D$ , where, for UV production, the dilution factor  $D \propto s_I^2 V_{PQ}(1, T_R)$  for  $(T_R > 10^{10} \text{ GeV}, T_R < 10^{10} \text{ GeV})$ . For UV axino production,  $Y_{\tilde{a}} \propto (T_R/V_{PQ}^2, 1)$ , with the constant value applying only if the equilibrium abundance is reached, which happens above and to the left of the dashed line. For  $T_R > 10^{11}$  GeV, the contour for  $s_I = 10^{18}$  GeV is vertical, corresponding to an equilibrium axino abundance, while the contours with  $s_I = 10^{15}, 3 \times 10^{16}$  GeV have  $T_R \propto V_{PQ}^3$ , and those with  $s_I = V_{PQ}$  are steeper with  $T_R \propto V_{PQ}^5$ . For  $10^6 \text{ GeV} < T_R < 10^{10} \text{ GeV}$ , both  $Y_{\tilde{a}}$  and  $D$  are



## High Scale mediation: DFSZ<sub>+</sub>

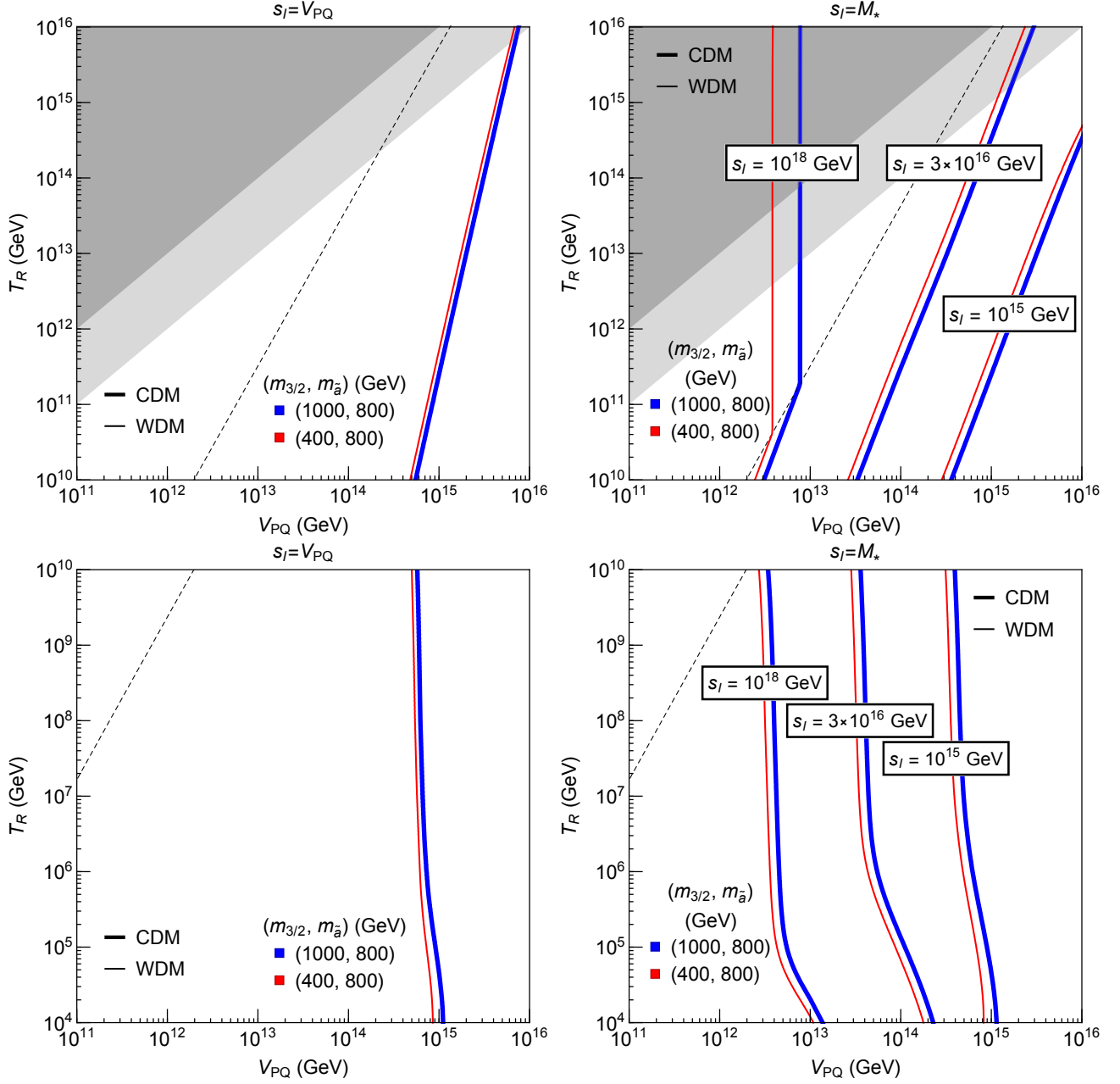


Figure 10: Contours of  $\Omega h^2 = 0.11$  from Axino freeze-in, Axino UV, and Gravitino UV production. We fix  $q_\mu = 2$ ,  $\mathcal{D} = 4$ ,  $\tan \beta = 2$ , and  $M_2/2 = M_1 = \mu = 1$  TeV and  $m_s = 300$  GeV. The top (bottom) row is for the cosmology with  $T_R \gtrsim (\lesssim) 10^{10}$  GeV discussed in Sec. 2.1 (Sec. 2.2).

## High Scale mediation: DFSZ<sub>+</sub> + Neutralino LOSP

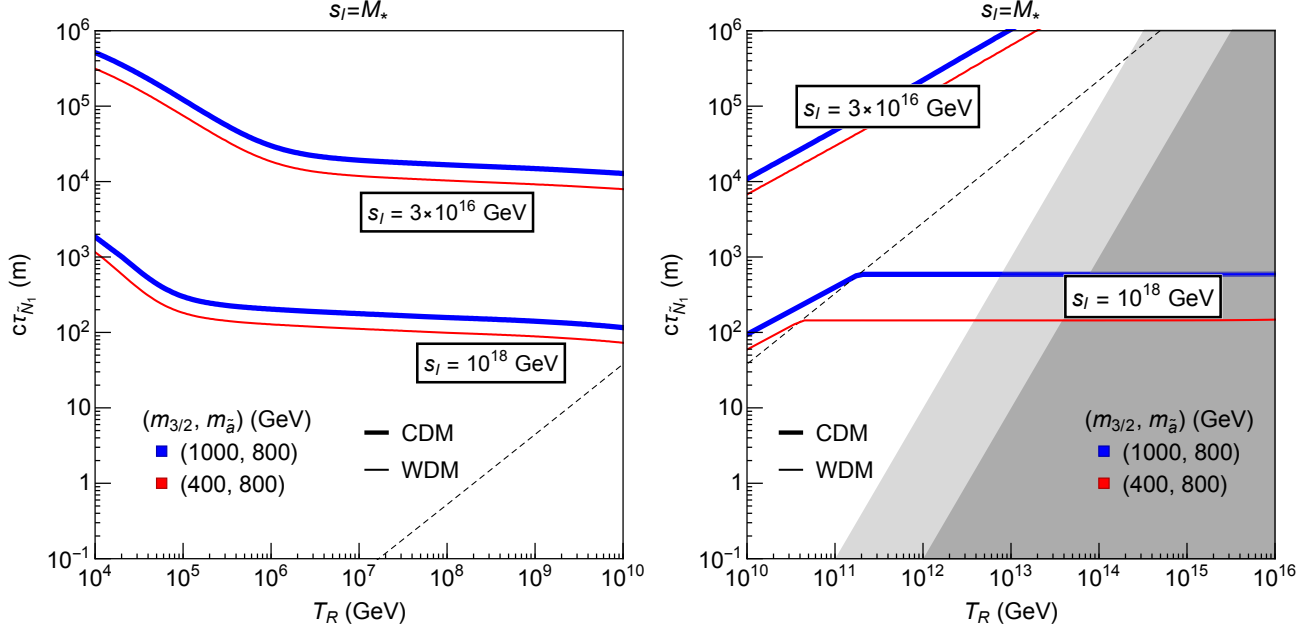


Figure 11: The decay length of the neutralino LOSP to the axino and the Higgs/Z boson, predicted from the  $\Omega h^2 = 0.11$  contours of Fig. 10. We fix  $q_\mu = 2$ ,  $\mathcal{D} = 4$ ,  $\tan \beta = 2$ , and  $M_2/2 = M_1 = \mu = 1$  TeV and  $m_s = 300$  GeV. The left (right) panel is for the cosmology with  $T_R \lesssim (\gtrsim) 10^{10}$  GeV discussed in Sec. 2.2 (Sec. 2.1).

linear in  $T_R$ , so that the contours are vertical. At very low  $T_R$  the contours become sloped as the axino yield becomes dominated by freeze-in; in this low  $T_R$  region they are identical to the curves in Fig. 8.

In Fig. 11, we predict the neutralino LOSP decay length, Eq. (4.6), from the values of  $V_{PQ}$  fixed by the observed dark matter abundance, in a way completely analogous to Fig. 9, with the left (right) panel for  $T_R$  less (greater) than  $10^{10}$  GeV. The key feature in DFSZ<sub>+</sub> is that, for all  $T_R > 10^6$  GeV, UV axino production dominates dark matter production and hence, compared to DFSZ<sub>0</sub>, more dilution (i.e. higher  $s_I$ ) is required for a given  $V_{PQ}$ . Fig. 11 shows that for  $s_I$  of order, or larger, than the scale of supersymmetric grand unification, displaced vertices should be observable at LHC. For fixed  $T_R$  and  $s_I$ , the decay length scales as  $m_{LSP}^{2/3}$ , unless the axino abundance from UV scattering reaches equilibrium, when it scales as  $m_{LSP}^2$ .

## 4.2 Low Scale or “Gauge” Mediation

### 4.2.1 The DFSZ<sub>0</sub> Theory

Dark matter production in DFSZ<sub>0</sub> theories is dominantly from axino freeze-in and Gravitino UV production as explained in Sec. 4.1.1. Here we are concerned with Low Scale mediation of

### Low Scale mediation: DFSZ<sub>0</sub>

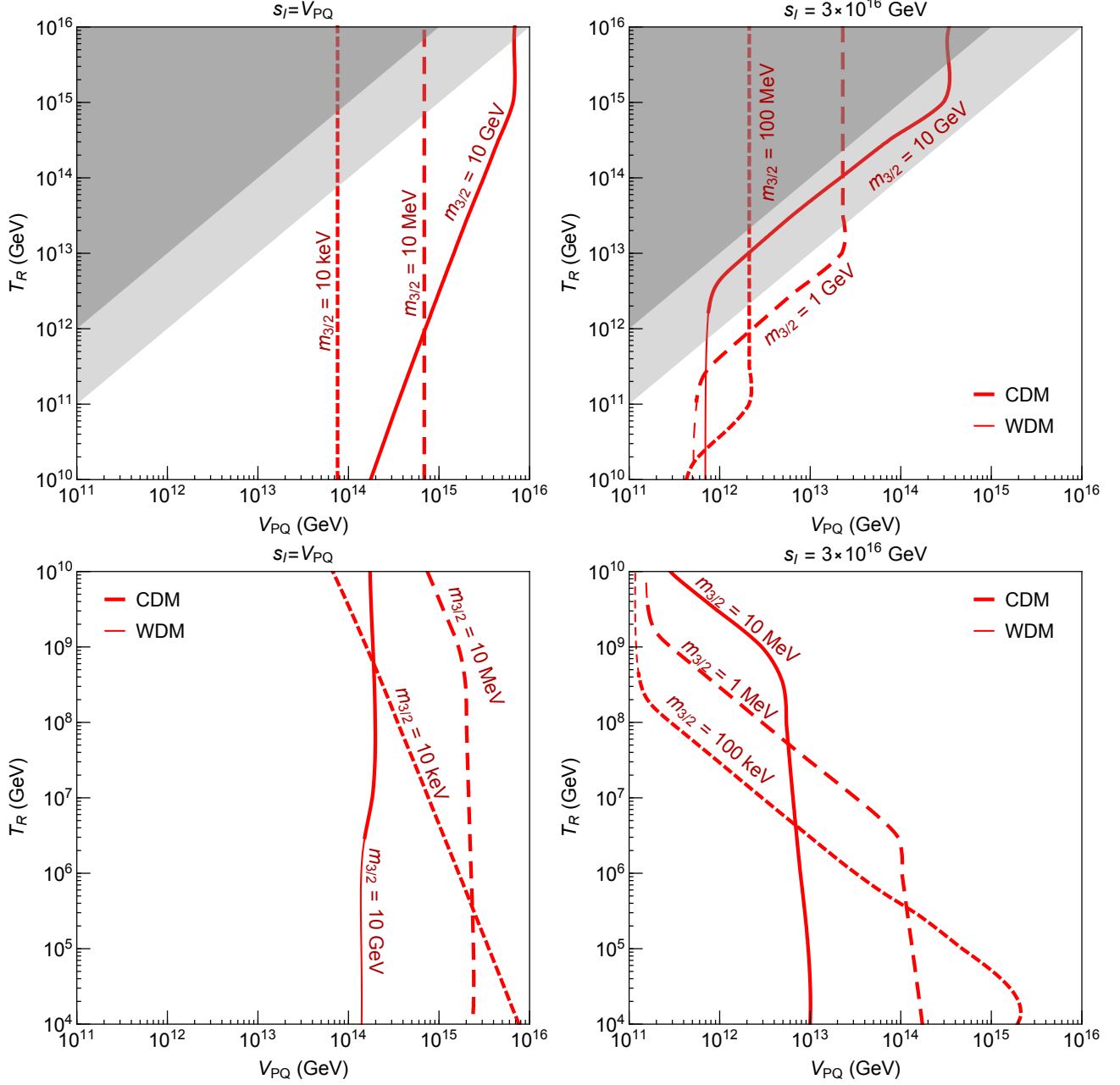


Figure 12: Contours of  $\Omega h^2 = 0.11$  from Axino freeze-in and Gravitino UV production. We fix  $q_\mu = 2$ ,  $\mathcal{D} = 4$ ,  $\tan \beta = 2$ ,  $M_2/2 = M_1 = \mu = 1$  TeV, and  $m_s = 300$  GeV. The top (bottom) row is for the cosmology with  $T_R \gtrsim (\lesssim) 10^{10}$  GeV discussed in Sec. 2.1 (Sec. 2.2).

## Low Scale mediation: DFSZ<sub>0</sub> + Neutralino LOSP

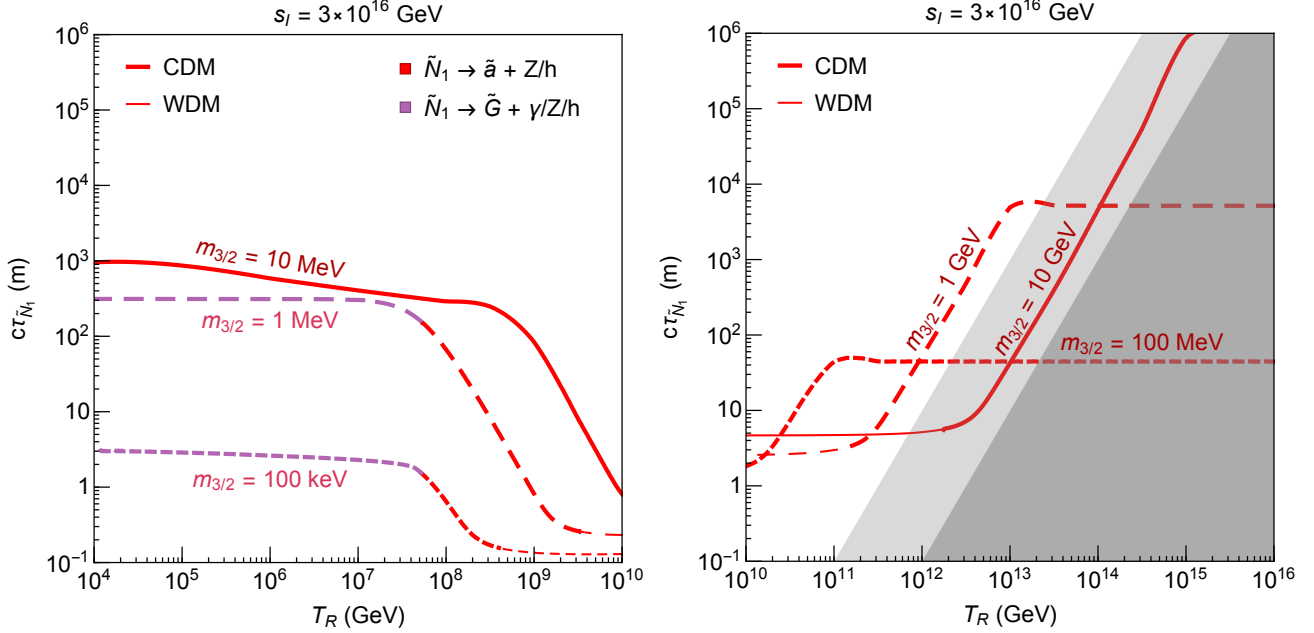


Figure 13: The decay length of the neutralino LOSP to the axino + h/Z (red) or to the gravitino +  $\gamma$ /Z (pink), predicted from the  $\Omega h^2 = 0.11$  contours of Fig. 12. We fix  $q_\mu = 2$ ,  $\mathcal{D} = 4$ ,  $\tan \beta = 2$ , and  $M_2/2 = M_1 = \mu = 1$  TeV and  $m_s = 300$  GeV. The left (right) panel is for the cosmology with  $T_R \lesssim (\gtrsim) 10^{10}$  GeV discussed in Sec. 2.2 (Sec. 2.1).

supersymmetry breaking, as in gauge mediation, and hence take the gravitino to be the LSP. Axinos produced from freeze-in decay and produce a warm component of gravitino dark matter.

In Fig. 12, we show contours of  $\Omega_{3/2} h^2 = 0.11$ . Following the same setup as in Figs. 8 and 10, the thin (thick) parts of the curves indicate LSP (NLSP) production domination and the gray region is excluded because of a post-inflationary cosmology. The upper (lower) panels are for the cosmology of  $T_R$  greater (lower) than  $10^{10}$  GeV discussed in Sec. 2.1 (Sec. 2.2). The left (right) panels assume  $s_I = V_{PQ}$  ( $M_* = 3 \times 10^{16}$  GeV). It is important to remember that the dilution factor is larger for larger  $V_{PQ}$ .

Gravitino UV production given by Eq. (3.13) is much enhanced for low  $m_{3/2}$ . For low enough  $m_{3/2}$  and high enough  $T_R$ , gravitino UV production is so large that gravitinos become thermalized. In this case, the thermal abundance is given by Eq. (3.12), independent of  $m_{3/2}$  and  $T_R$ . In the upper panels, the vertical thick parts correspond to this thermal gravitino production. While  $T_R$  decreases, the gravitino may become non-thermal and follows Eq. (3.13), which then decreases with  $T_R$ . This non-thermal gravitino is labeled by sloped parts of the thick curves in the upper panels. Lastly, the thin vertical curves label the axino FI domination. Since axino FI production in Eqs. (3.7) and (3.9) is independent of  $m_{\tilde{a}}$ , the result generically applies for any  $m_{\tilde{a}}$  between 650 GeV – 1 TeV as required by the free-streaming length for cold dark matter and

neutralino decay kinematics respectively.

In the lower panels, the dilution factor in the cosmology described in Sec. 2.2 scales linearly with  $T_R$ . Therefore, the curves for thermal gravitino production (with a constant undiluted yield) are now at a slope. On the other hand, non-thermal gravitino UV production is close to being proportional to  $T_R$  as well, and with dilution, the final yield becomes independent of  $T_R$ , corresponding to the vertical thick parts. Lastly, the axino FI production dominates at the vertical thin parts of the curves.

In Fig. 13, the LOSP decay lengths can again be predicted from Eq. (4.6) with the values of  $V_{PQ}$  that give the observed dark matter abundance. The left (right) panel corresponds to the cosmology of  $T_R$  less (greater) than  $10^{10}$  GeV discussed in Sec. 2.2 (Sec. 2.1). It is worth noting that we are choosing different values of the gravitino mass in these two panels to demonstrate interesting LOSP decay signals for the relevant regions. In particular, we open up a new decay channel when the gravitino mass is less than  $\mathcal{O}(1)$  MeV– the neutralino LOSP decays to the gravitino and  $\gamma/h/Z$ . This decay channel with the rate given in Eq. (4.7) dominates in the purple portions of the curves. As in Fig. 12, the thin parts of the lines are dominated by the axino FI contribution and lead to warm dark matter because of the late axino decay to axions and gravitinos. For clarity, only one value of  $s_I$  is shown but there exists a set of correlated  $m_{3/2}$  and  $s_I$  that can lead to LOSP displaced signals. In particular, a low  $m_{3/2}$  enhances the production and thus requires a larger  $s_I$  for dilution. However, once  $m_{3/2}$  is sufficiently low for the gravitino to be thermalized, any lower  $m_{3/2}$  results in a decrease in its energy density and a smaller  $s_I$  is needed. This is remarkable that the LOSP decay lengths for low  $m_{3/2}$  are

#### 4.2.2 The DFSZ<sub>+</sub> Theory

Here we have a new axino UV contribution in addition to those of axino FI and gravitino UV discussed in Sec. 4.2.1 for the DFSZ<sub>0</sub> theories. The total dark matter abundance is shown in Fig. 14 as contours of  $\Omega h^2 = 0.11$ .

We observe that axino FI is always subdominant in the high  $T_R$  regimes. Therefore, in discussing the upper panels of Fig. 14, we only need to identify axino UV and gravitino UV. Since the thick parts of the curves indicate gravitino UV domination, the features of these parts are identical to those in Fig. 12. The new features are in the thin parts. In the upper panels, the vertical thin curves correspond to axino UV thermal abundance given by Eq. (3.12). In the lower left panel, since the dilution factor becomes unity in regions where  $T_R \lesssim 10^{5-6}$  GeV and  $V_{PQ} \lesssim 10^{14-15}$  GeV, the gravitino UV decreases with  $T_R$  and the curve starts to follow axino FI contribution in the vertical thin parts. As axino FI and UV production in Eqs. (3.7) and (3.9) and Eq. (3.11) is independent of  $m_{\tilde{a}}$ , the result generically applies for any  $m_{\tilde{a}}$  between 650 GeV – 1 TeV as required by the free-streaming length for cold dark matter and neutralino decay kinematics, respectively.

Finally, we also make predictions of neutralino LOSP decay lengths in Fig. 15. Similar to Fig. 13, the relevant decay modes are  $\tilde{N}_1 \rightarrow \tilde{a}$  (red) and  $\tilde{N}_1 \rightarrow \tilde{G}$  (purple), with the latter dominating for low  $m_{3/2}$ . The prediction of the total decay rate, when dominated by  $\Gamma_{\tilde{N}_1 \rightarrow \tilde{G}}$ , depends on  $m_{3/2}$  and is insensitive to dark matter production and dilution. On the other hand,

### Low Scale mediation: DFSZ<sub>+</sub>

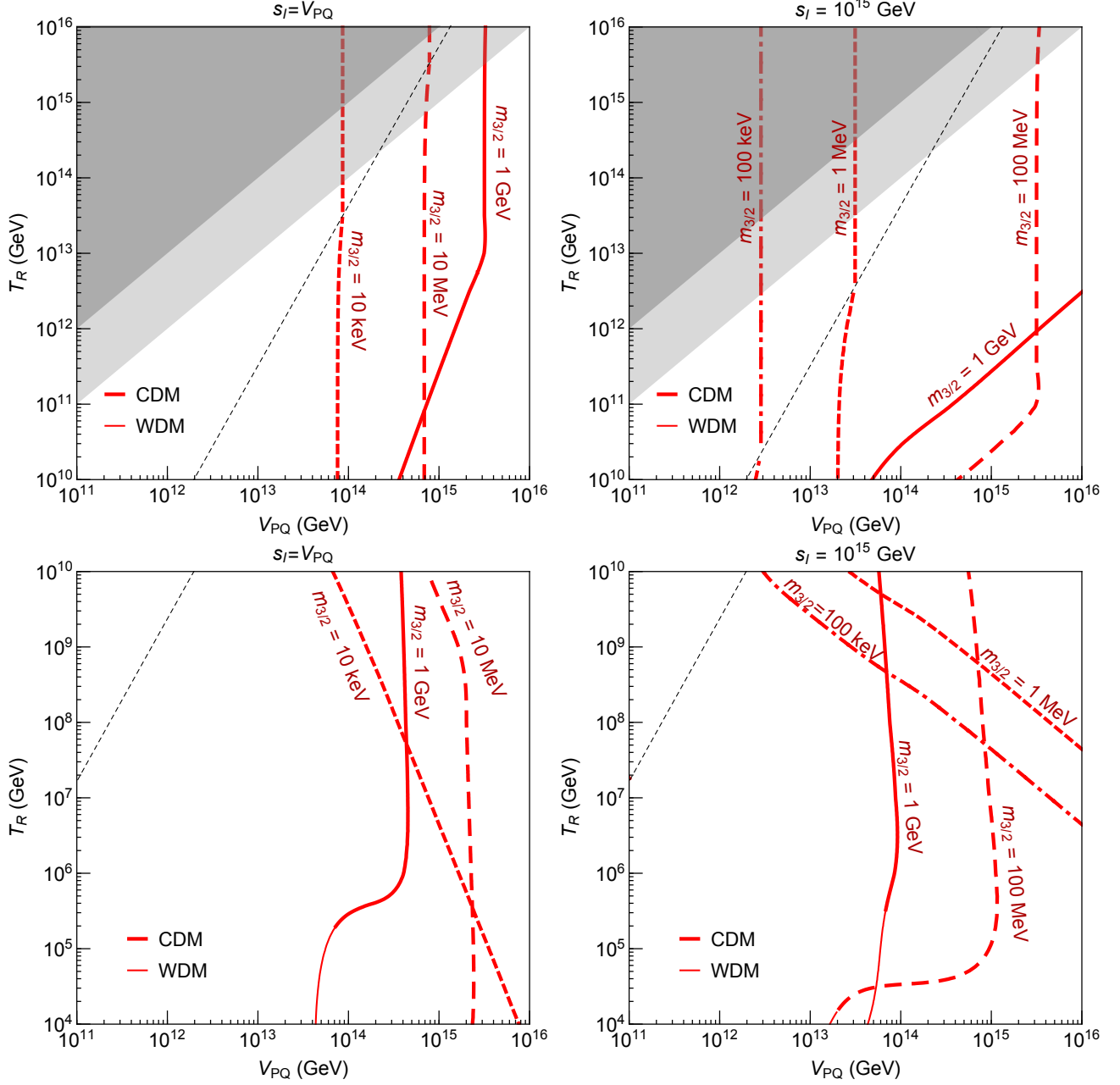


Figure 14: Contours of  $\Omega h^2 = 0.11$  from Axino freeze-in and Gravitino UV production. We fix  $q_\mu = 2$ ,  $\mathcal{D} = 4$ ,  $\tan \beta = 2$ , and  $M_2/2 = M_1 = \mu = 1 \text{ TeV}$  and  $m_s = 300 \text{ GeV}$ . The top (bottom) row is for the cosmology with  $T_R \gtrless 10^{10} \text{ GeV}$  discussed in Sec. 2.1 (Sec. 2.2).

## Low Scale mediation: DFSZ<sub>+</sub> + Neutralino LOSP

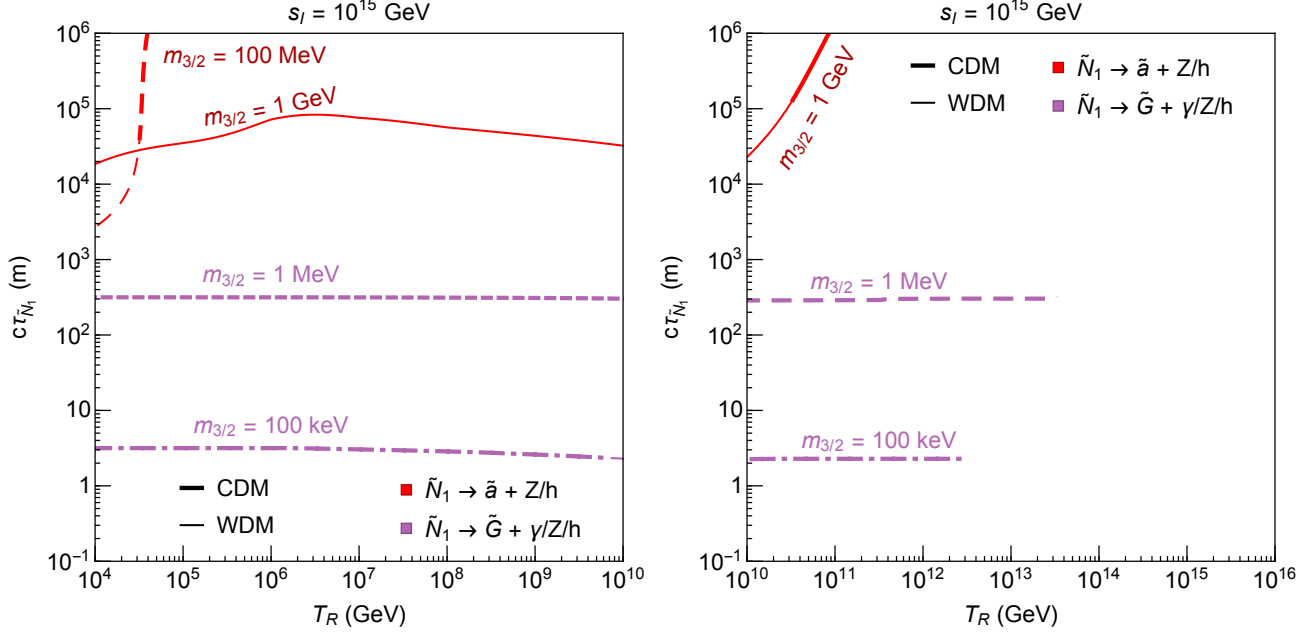


Figure 15: The decay length of the neutralino LOSP to the axino + h/Z (red) or to the gravitino +  $\gamma/Z$  (pink), predicted from the  $\Omega h^2 = 0.11$  contours of Fig. 14. We fix  $q_\mu = 2$ ,  $\mathcal{D} = 4$ ,  $\tan \beta = 2$ , and  $M_2/2 = M_1 = \mu = 1$  TeV and  $m_s = 300$  GeV. The left (right) panel is for the cosmology with  $T_R \lesssim (\gtrsim) 10^{10}$  GeV discussed in Sec. 2.2 (Sec. 2.1).

once  $m_{3/2}$  is sufficiently large,  $\tilde{N}_1 \rightarrow \tilde{a}$  dominates and the decay length prediction is set by the value of  $V_{PQ}$  that gives  $\Omega h^2 = 0.11$  in Fig. 14. The thin (thick) lines label warm (cold) dark matter. The left (right) panel corresponds to the low (high)  $T_R$  cosmology studied in Sec. 2.2 (Sec. 2.1). In the right panel, the purple curves are truncated on the right at the values of  $T_R$  where the curves enter the light gray excluded post-inflationary region in upper right panel of Fig. 14. It is worth noting that for clarity we only show the prediction for one value of  $s_I$  and there is a large set of parameters that lead to collider signals with viable cosmology.

### 4.3 Displaced Signals at Colliders: dependence on $(\mu, M_1, V_{PQ}, m_{3/2})$

In Figures 9, 11, 13, and 15 we show predictions for the neutralino decay length, following from the constraint  $\Omega h^2 = 0.11$ , in theories with High and Low Scale mediation for the particular point in supersymmetric parameter space of  $(\mu, M_1, \tan \beta) = (1 \text{ TeV}, 1 \text{ TeV}, 2)$ . Here we illustrate the variation in the decay lengths of Eq. (4.6) for the axino final state and Eqs. (B.26)–(B.29) for the gravitino final state as the parameter space changes. We still keep the unified gaugino mass relation,  $M_2 \simeq 2M_1$ . We compute the partial decay width  $\Gamma_{\tilde{N}_1 \rightarrow i}$  for the decay channel  $i = (\tilde{a}, \tilde{G})$ . In Fig. 16, for clarify we display  $\Gamma_{\tilde{N}_1 \rightarrow i}^{-1}$  in meters from each of the decay mode

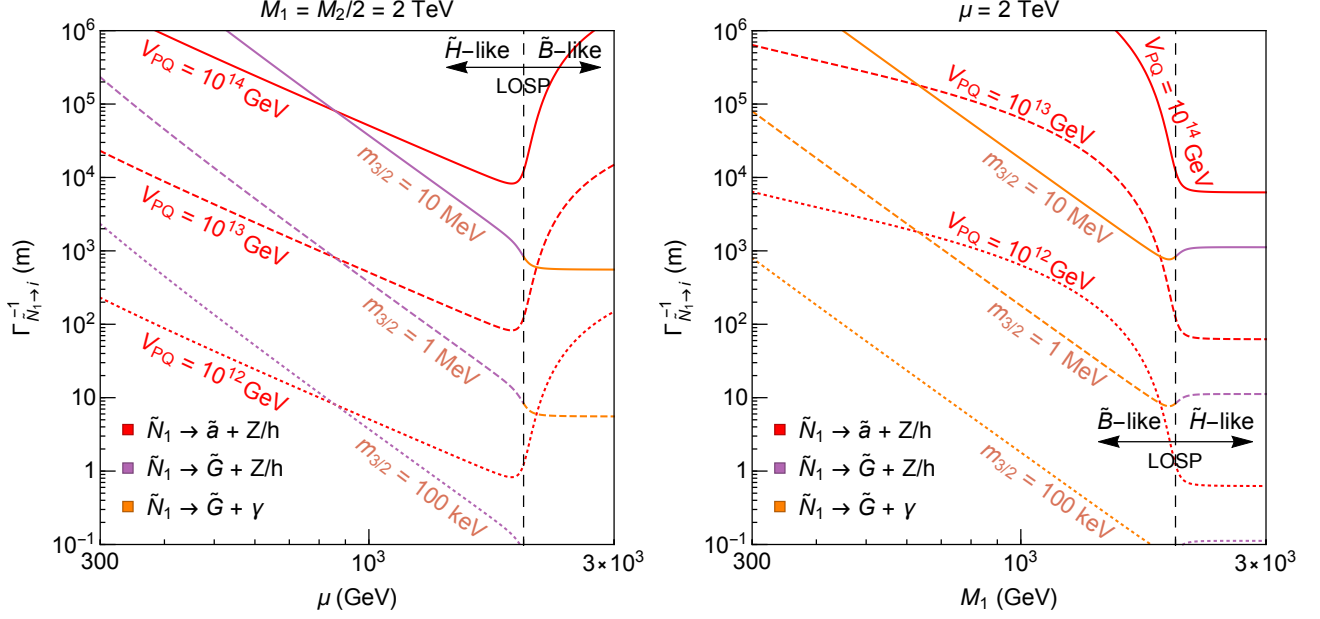


Figure 16: The neutralino LOSP inverse partial decay width  $\Gamma_{\tilde{N}_1 \rightarrow i}^{-1}$  ( $i = \tilde{a}, \tilde{G}$ ) as a function of  $\mu$  ( $M_1$ ) plane for fixed  $M_1$  ( $\mu$ ) in the left (right) panel, with  $q_\mu = 2$ ,  $\tan \beta = 2$ , and  $M_2 \simeq 2M_1$ . The decay length of  $\tilde{N}_1 \rightarrow \tilde{a}$  ( $\tilde{G}$ ) is proportional to  $V_{PQ}^2$  ( $m_{3/2}^2$ ), the chosen values of which are labeled by the solid/dashed/dotted curves in each panel. The colors indicate the predictions from the various decay channels. Once  $V_{PQ}$  and  $m_{3/2}$  are fixed, the overall decay length is determined by the decay channel that gives the smallest  $c\tau_{\tilde{N}_1}$  prediction.

$i$ , labeled by different colors. The decay length to  $\tilde{a}$  ( $\tilde{G}$ ) is proportional to  $V_{PQ}^2$  ( $m_{3/2}^2$ ). The overall LOSP decay length  $c\tau_{\tilde{N}_1} = (\sum_i \Gamma_{\tilde{N}_1 \rightarrow i})^{-1}$  is primarily given by the decay channel with the smallest  $\Gamma_{\tilde{N}_1 \rightarrow i}^{-1}$ . In the left (right) panel, we vary  $\mu$  ( $M_1$ ) while fixing  $M_1$  ( $\mu$ ). The change of behavior in the lifetime curves at  $\mu = 2$  TeV ( $M_1 = 2$  TeV) in the left (right) panel reflects the fact that the mixing factors in Eq. (4.6) and in Eqs. (B.26)–(B.29) drastically change as  $\mu$  becomes larger or smaller than  $M_1$ . The neutralino LOSP decay can lead to observable displaced signals at the LHC and future colliders over a remarkably wide range of parameter space.

## 5 Neutralino LSP from Axino Freeze-In

For a neutralino LSP, the usual freeze-out abundance is greatly diluted by decay of the saxion condensate. The dark matter abundance instead originates from the axino and gravitino production described in Sec. 3. Here we assume that axino freeze-in dominates, so that the UV processes depending on  $T_R$  are irrelevant. The axinos produced from freeze-in later decay to the LSP which, in the parameter space of interest, occurs after LSP freeze-out but before BBN. Note that the removal of the freeze-out contribution means there is no need to fine-tune



parameters as, for example, in the well-tempered neutralino scenario [48].

The decay rate in Eq. (B.14) (inverse decay rate in Eq. (B.15)) depends on the mass of the decaying  $\chi_i$  (the mass of axino) and therefore the dark matter abundance requires the knowledge of the mass spectrum of neutralinos, charginos, and axinos. For a neutralino LSP, either only the inverse decay or both the decay and inverse decay processes can be active depending on where the axino mass sits in the  $\chi$  spectrum. Nevertheless, for a general mass spectrum, we expect the yield of axino to lie in between the red and orange curves in Fig. 4, the two extreme cases where all  $\chi$ 's are heavier or lighter than the axino. This axino yield can also be thought of as the neutralino LSP yield because each axino eventually decays to one LSP. Based on Fig. 4, for weak scale LSP masses,  $V_{PQ}$  is expected to be  $10^{13-14}$  GeV ( $10^{11-12}$  GeV) for the case of  $s_I = V_{PQ}$  ( $\geq 10^{17}$  GeV).

The effects of neutralino and chargino mass parameters are further studied in Fig. 17. In particular, we show contours of  $V_{PQ}$  that give the observed dark matter abundance in the  $M_1$  and  $\mu$  plane for  $M_2 = 3/(5 \tan^2 \theta_W) M_1 \simeq 2M_1$  and fixed  $\tan \beta = 2$ . The top and bottom rows assume  $\mu > m_{\tilde{a}} > M_1$  and  $m_{\tilde{a}} > \mu$  respectively, while the left and right columns use  $s_I = V_{PQ}$  and  $M_*$ . The blue (white) region labels the parameter space with the Higgsino-like and Bino-like LSP. When the gaugino masses are well separated from those of Higgsinos, the gaugino couplings to the axino become very suppressed. This implies that the dominant freeze-in process in the top (bottom) row is the decay (inverse decay) involving the Higgsino, except at the interface between the white and blue shadings where both are comparable. The bino coupling suppression explains why the dark matter abundance is independent of  $M_1$  in the blue regions. These panels show that our prediction of  $V_{PQ}$  is insensitive to the detailed mass spectrum of  $\chi$  but mainly determined by the saxion initial oscillation amplitude  $s_I$ .

## Acknowledgments

We acknowledge useful conversations with Marcin Badziak, Kimberly Boddy, and Keisuke Harigaya. This work was supported in part by the Director, Office of Science, Office of High Energy and Nuclear Physics, of the US Department of Energy under Contract DE-AC02-05CH11231 and by the National Science Foundation under grants PHY-1002399 and PHY-1316783. R.C. is supported by the National Science Foundation Graduate Research Fellowship under Grant No. DGE 1106400. F.D. is supported by the U.S. Department of Energy grant number DE-SC0010107.

## A Axion Supermultiplet Interactions

In this Appendix we develop a general framework to describe effective interactions of the axion supermultiplet. We consider both self-interactions and couplings to MSSM fields. In the next Appendix, we use these results to compute the decay widths used in this work.

At energies below the PQ breaking scale the theory is still approximately supersymmetric. We assume the PQ symmetry to be broken by a set of chiral superfields  $\Phi_i$ , which we expand

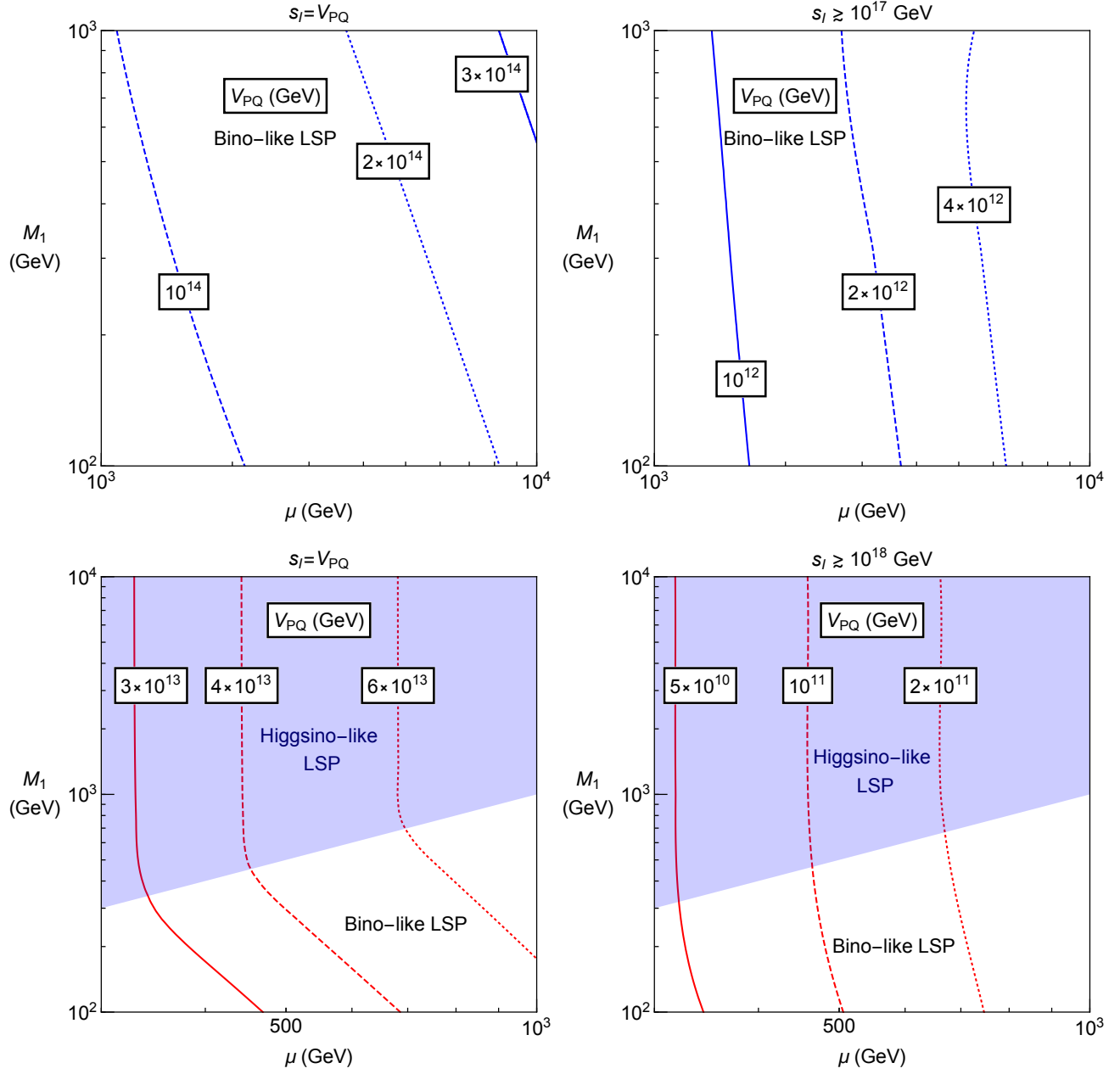


Figure 17: Contours of  $V_{PQ}$  giving the observed abundance of neutralino LSP dark matter from axino freeze-in, where  $m_{\tilde{a}} = 1.5$  (2 TeV) for the top (bottom) rows and  $\tan \beta = 2$ .

around their vacuum expectation values (vev)

$$\Phi_i = v_i \exp \left[ q_i \frac{A}{V_{PQ}} \right] . \quad (\text{A.1})$$

The axion  $a$  fills the supermultiplet  $A$  as explicitly given in Eq. (1.1), together with its superpartners, the saxion  $s$  and the axino  $\tilde{a}$ . We normalize the PQ charges  $q_i$  of the PQ breaking fields in such a way that they are all integers and  $|q_i|$  as small as possible. Within this convention, the effective PQ breaking scale is defined as follows

$$V_{PQ}^2 = \sum_i q_i^2 v_i^2 . \quad (\text{A.2})$$

The effect of a PQ rotation with an angle  $\alpha$  on the axion superfield is the following

$$A \rightarrow A + i\alpha V_{PQ} . \quad (\text{A.3})$$

The interactions of the axion supermultiplet are significantly constrained by this shift invariance.

## A.1 Color Anomaly

The PQ symmetry is broken by a color anomaly, which generates the low-energy interaction

$$\mathcal{L}_{AWW} = -\frac{g_3^2 N_{\text{DW}}}{32\pi^2 v_{PQ}} \int d^2\theta A W^\alpha W_\alpha + \text{h.c.} \quad (\text{A.4})$$

between the axion superfield  $A$  and the supersymmetric QCD field strength  $W^\alpha$ . The domain wall number  $N_{\text{DW}}$  appearing in the above expression is the QCD anomaly coefficient of the PQ symmetry. Finally, we define the axion decay constant

$$f_a = \frac{\sqrt{2}}{N_{\text{DW}}} V_{PQ} . \quad (\text{A.5})$$

Upon expanding in component fields the supersymmetric expression in Eq. (A.4), we identify the effective interaction between the axion  $a$  and the QCD field strength  $G$

$$\mathcal{L}_{aG\tilde{G}} = \frac{g_3^2}{32\pi^2} \frac{a}{f_a} G^{\mu\nu} \tilde{G}_{\mu\nu} . \quad (\text{A.6})$$

## A.2 Supersymmetric Interactions

We assume the fields in Eq. (A.1) to be canonically normalized, and the Kähler potential reads

$$K = \sum_i \Phi_i^\dagger \Phi_i = \sum_i v_i^2 \exp \left[ q_i \left( \frac{A + A^\dagger}{V_{PQ}} \right) \right] = A^\dagger A + \frac{1}{2} \sum_i \frac{q_i^3 v_i^2}{V_{PQ}^3} A^\dagger A (A + A^\dagger) + \dots \quad (\text{A.7})$$

This function only depends on the PQ invariant combination  $A + A^\dagger$ , consistently with the invariance under the shift in Eq. (A.3). The axion superfield  $A$  is canonically normalized.

Holomorphy and PQ invariance forbid superpotential self-interactions for  $A$ . However, the axion superfield  $A$  can appear in the superpotential of DFSZ theories, where the  $\mu$  term is PQ charged. We are allowed to write the PQ invariant operator

$$W = \mu \exp \left[ q_\mu \frac{A}{V_{PQ}} \right] H_u H_d = \mu H_u H_d + q_\mu \frac{\mu}{V_{PQ}} A H_u H_d + \dots \quad (\text{A.8})$$

Here, we denote  $q_\mu$  as the model-dependent PQ charge of the  $\mu$  term.

### A.3 SUSY breaking Interactions

Finally, we account for SUSY breaking. We find it convenient to employ the non-linear field

$$X = \left( \theta + \frac{\tilde{G}}{\sqrt{2}F} \right)^2 F, \quad (\text{A.9})$$

where  $F$  is the SUSY breaking scale and  $\tilde{G}$  is the associated goldstino.

SUSY breaking is transmitted to the PQ sector through the higher dimensional operator

$$K_{SUSY} = c_{AAX} \frac{(A + A^\dagger)^2 (X + X^\dagger)}{M_{\text{mess}}}, \quad (\text{A.10})$$

with  $M_{\text{mess}}$  the mass scale of the particles coupling the two sectors. We expect this operator to be generated by Planck scale dynamics [12], and therefore we have the upper limit on the mediation scale  $M_{\text{mess}} \lesssim M_{\text{Pl}}$ . A consequence of this operator is a contribution to the axino mass

$$\int d^4\theta K_{SUSY} = -c_{AAX} \frac{F}{M_{\text{mess}}} \tilde{a}\tilde{a} = -\frac{1}{2} (2\sqrt{3} c_{AAX} \frac{M_{\text{Pl}}}{M_{\text{mess}}} m_{3/2}) \tilde{a}\tilde{a} + \dots, \quad (\text{A.11})$$

where we have used the known relation  $m_{3/2} = F/(\sqrt{3}M_{\text{Pl}})$ . As discussed in the main text of this work, it is not natural to have an axino much lighter than the gravitino, unless there is some good reason to suppress the size of the coefficient  $c_{AAX}$  (e.g. sequestering).

Furthermore, we also require the presence of an effective  $B\mu$  term necessary for a successful electroweak symmetry breaking

$$W_{SUSY} = -c_B X \exp \left[ q_\mu \frac{A}{V_{PQ}} \right] H_u H_d, \quad (\text{A.12})$$

with  $c_B F = B\mu$ .

## B Decay Widths

Saxion decays are responsible for reheating the universe and producing dark radiation. Decays and inverse decays of neutralinos and charginos generate an axino freeze-in abundance. The axino decay to the gravitino creates a warm DM population and vice versa. Finally, neutralino decays to axino or gravitino lead to displaced collider events. We compute the decay widths for all these processes, using the interactions derived above.

### B.1 Saxion Decays

The saxion can decay to three possible final states: axions, axinos and Higgs bosons. The first two processes are mediated by the axion multiplet self-interactions, more specifically the cubic Kähler potential term in Eq. (A.7). Once we expand in component fields, we find the operators

$$\mathcal{L}_{saa, s\tilde{a}\tilde{a}} = -\frac{\kappa}{\sqrt{2}V_{\text{PQ}}} s \partial^\mu a \partial_\mu a + \frac{\kappa}{\sqrt{2}V_{\text{PQ}}} s m_{\tilde{a}} (\tilde{a}\tilde{a} + \tilde{a}^\dagger \tilde{a}^\dagger) . \quad (\text{B.1})$$

Here, we define the dimensionless parameter  $\kappa = \sum_i q_i^3 v_i^2 / V_{\text{PQ}}^2$ . For models with only a single PQ breaking field, or theories with more than one but all with the same PQ charge, we have  $\kappa = 1$ . In more general cases  $\kappa$  is a free parameter. If  $\kappa$  is non-zero, axinos can be copiously produced from saxion decays. Neglecting the final state masses, the decay widths are

$$\Gamma_{s \rightarrow aa} = \frac{\kappa^2 m_s^3}{64\pi V_{\text{PQ}}^2} , \quad (\text{B.2})$$

$$\Gamma_{s \rightarrow \tilde{a}\tilde{a}} = \frac{\kappa^2 m_{\tilde{a}}^2 m_s}{8\pi V_{\text{PQ}}^2} . \quad (\text{B.3})$$

More importantly for the reheating process, the saxion can decay to Higgs bosons and longitudinal electroweak gauge bosons. These decays are mediated from the supersymmetric interactions arising from the superpotential in Eq. (A.8) as well as the SUSY breaking interactions arising from Eq. (A.12). The resulting scalar potential interactions are

$$V_{sHH} = \sqrt{2} q_\mu \frac{\mu^2}{V_{\text{PQ}}} s \left( H_u^\dagger H_u + H_d^\dagger H_d \right) + q_\mu \frac{B}{V_{\text{PQ}}} \frac{s}{\sqrt{2}} (H_u H_d + \text{h.c.}) . \quad (\text{B.4})$$

The Higgs doublets  $H_u$  and  $H_d$  contain three Goldstones ( $G^\pm$  and  $G^0$ ) providing electroweak gauge bosons longitudinal modes, two CP-even ( $h$  and  $H$ ) and one CP-odd ( $A$ ) neutral scalars and one charged scalar ( $H^\pm$ ). We consider the decoupling limit where the non-SM fields are heavy. In such a limit, we find it convenient to introduce the doublets

$$H_{\text{SM}} = \begin{pmatrix} G^+ \\ v + \frac{h+iG^0}{\sqrt{2}} \end{pmatrix} , \quad H_{\text{Heavy}} = \begin{pmatrix} \frac{H+iA}{\sqrt{2}} \\ H^- \end{pmatrix} . \quad (\text{B.5})$$

The SM-like Higgs boson  $h$  lives within the multiplet  $H_{\text{SM}}$ , which takes the electroweak symmetry breaking vev. The decoupling limit holds as long as  $m_A \gg m_Z$ , and in such a limit the connection between gauge eigenstates and mass eigenstates reads

$$H_u = \sin \beta H_{\text{SM}} + \cos \beta H_{\text{Heavy}}^{(c)} , \quad (\text{B.6})$$

$$H_d = \cos \beta H_{\text{SM}}^{(c)} + \sin \beta H_{\text{Heavy}} , \quad (\text{B.7})$$

where we introduce the ratio between the two vevs  $\tan \beta = v_u/v_d$  and with  $H_i^{(c)} = i\sigma^2 H_i^*$ . We report here the decay width in such a decoupling limit and for large  $\tan \beta$  (for more general expressions see App. A of Ref. [20])

$$\Gamma_{s \rightarrow \text{visible}} = \mathcal{D} \frac{q_\mu^2 \mu^4}{16\pi m_s V_{\text{PQ}}^2} . \quad (\text{B.8})$$

Here,  $\mathcal{D}$  counts the number of kinematically allowed final state particles. For a SM Higgs sector we have  $\mathcal{D} = 4$ , whereas  $\mathcal{D} = 8$  for the full MSSM Higgs sector.

## B.2 Neutralino and Chargino Decays to Axinos

We start by defining the mixing matrices for the MSSM neutralinos and charginos. We collect the neutralinos into the four-dimensional array

$$\tilde{\chi} = \begin{pmatrix} \tilde{B} & \tilde{W}^3 & \tilde{h}_d^0 & \tilde{h}_u^0 \end{pmatrix} , \quad (\text{B.9})$$

and the connection with mass eigenstates  $\tilde{N}_i$  is achieved through the rotation

$$\tilde{\chi} = R \tilde{N} , \quad (R^\dagger R = R R^\dagger = 1) . \quad (\text{B.10})$$

Likewise, we group the charginos into the two different two-dimensional arrays

$$\tilde{\psi}^+ = \begin{pmatrix} \tilde{W}^+ \\ \tilde{h}_u^+ \end{pmatrix} , \quad \tilde{\psi}^- = \begin{pmatrix} \tilde{W}^- \\ \tilde{h}_d^- \end{pmatrix} , \quad (\text{B.11})$$

containing positively and negatively charged states, respectively. We separately rotate the two chargino arrays

$$\tilde{C}^+ = V^\dagger \tilde{\psi}^+ , \quad (V^\dagger V = V V^\dagger = 1) , \quad (\text{B.12})$$

$$\tilde{C}^- = U^\dagger \tilde{\psi}^- , \quad (U^\dagger U = U U^\dagger = 1) , \quad (\text{B.13})$$

and as expected we find that the mass eigenvalues for the two arrays are the same. The positively and negatively charged mass eigenstates fill a Dirac fermion.

For neutralinos decays and inverse decays we have

$$\Gamma_{\tilde{N}_i \rightarrow \tilde{a}H} = \left( \frac{q_\mu \mu}{V_{\text{PQ}}} \right)^2 \frac{m_{\tilde{N}_i}}{16\pi} (|s_\beta R_{3i}|^2 + |c_\beta R_{4i}|^2) , \quad (\text{B.14})$$

$$\Gamma_{\tilde{a} \rightarrow \tilde{N}_i H} = \left( \frac{q_\mu \mu}{V_{\text{PQ}}} \right)^2 \frac{m_{\tilde{a}}}{16\pi} (|s_\beta R_{3i}|^2 + |c_\beta R_{4i}|^2) , \quad (\text{B.15})$$

where  $R$  is the rotation matrix defined in Eq. (B.10). Likewise, for charginos

$$\Gamma_{\tilde{C}_i^\pm \rightarrow \tilde{a}\phi_+} = \left( \frac{q_\mu \mu}{V_{\text{PQ}}} \right)^2 \frac{m_{\tilde{C}_i^\pm}}{32\pi} (|s_\beta U_{2i}|^2 + |c_\beta V_{2i}|^2) , \quad (\text{B.16})$$

$$\Gamma_{\tilde{a} \rightarrow \tilde{C}_i^\pm \phi_+} = \left( \frac{q_\mu \mu}{V_{\text{PQ}}} \right)^2 \frac{m_{\tilde{a}}}{32\pi} (|s_\beta U_{2i}|^2 + |c_\beta V_{2i}|^2) , \quad (\text{B.17})$$

with  $U$  and  $V$  defined in Eqs. (B.12) and (B.13).

### B.3 Gravitino Decays

Gravitino decays are mediated by the Planck suppressed supergravity operators [49]

$$\mathcal{L}_\psi = - \frac{i}{2M_{\text{Pl}}} \mathcal{J}^\mu \psi_\mu + \text{h.c.} , \quad (\text{B.18})$$

$$\mathcal{J}^\mu = \sqrt{2} \sigma^\nu \bar{\sigma}^\mu \chi \partial_\nu \phi^\dagger - \sigma^{\alpha\beta} \sigma^\mu \lambda^{a\dagger} F_{\alpha\beta}^a , \quad (\text{B.19})$$

The supercurrent  $\mathcal{J}^\mu$  contains both chiral superfields with components  $(\phi, \chi)$  as well as gauge superfields with components  $(V, \lambda)$ . Here,  $F$  is the field strength of the vector field  $V$ . The gravitino decay width to chiral multiplet components reads

$$\Gamma_{\psi \rightarrow \phi \chi} = N_c^{(\phi)} \frac{m_{3/2}^3}{384\pi M_{\text{Pl}}^2} , \quad (\text{B.20})$$

where we neglect the final state masses and the color factor accounts for a decay to a quark/squark pair ( $N_c^{(\text{quarks})} = 3$ ). Likewise, the decay width to gauge multiplet components results in

$$\Gamma_{\psi \rightarrow V \lambda} = N_c^{(V)} \frac{m_{3/2}^3}{32\pi M_{\text{Pl}}^2} . \quad (\text{B.21})$$

Here, the multiplicity factor is  $(8, 3, 1)$  for the cases of final state (gluino, wino, bino).

### B.4 Axino and Neutralino decays to gravitinos

In the last part of this Appendix, we consider decays to final states involving gravitino. We assume the gravitino to be much lighter than the decaying particle, so that we can approximate

the process with decays to longitudinal gravitinos, in accordance with the equivalence theorem. The process is correctly described by the effective Lagrangian <sup>5</sup>

$$\mathcal{L}_\psi = -\frac{1}{F}\tilde{G}\partial_\mu J^\mu + \text{h.c.} , \quad (\text{B.22})$$

$$J^\mu = \sigma^\nu \bar{\sigma}^\mu \chi \partial_\nu \phi^\dagger - \frac{1}{\sqrt{2}} \sigma^{\alpha\beta} \sigma^\mu \lambda^{a\dagger} F_{\alpha\beta}^a , \quad (\text{B.23})$$

where we consider again both chiral  $(\phi, \chi)$  and vector  $(V, \lambda)$  supermultiplets. We note that the above interactions can also be derived from the full supergravity result in Eq. (B.18), by identifying the longitudinal component of the gravitino

$$\psi_\mu \rightarrow i \sqrt{\frac{2}{3}} \frac{\partial_\mu \tilde{G}}{m_{3/2}} . \quad (\text{B.24})$$

Upon using the Goldstino equations of motion [52, 53] and the relation  $m_{3/2} = F/(\sqrt{3}M_{\text{Pl}})$ , we recover the interaction between the Goldstino and the flat-space global SUSY supercurrent.

The first case we discuss is the axino decay to axion and gravitino. The associated axino decay to saxion and gravitino is assumed to be kinematically forbidden. Upon using the general supercurrent result, and accounting for only the axion final state, we find

$$\Gamma_{\tilde{a} \rightarrow \tilde{G} a} = \frac{m_{\tilde{a}}^5}{96\pi m_{3/2}^2 M_{\text{Pl}}^2} \quad (\text{B.25})$$

The last cases we discuss are the ones relevant for displaced collider signatures. We only consider decays of the lightest neutralino  $\tilde{N}_1$ , since every other R-odd particle produced at collider will promptly decay to it. The mass eigenstate  $\tilde{N}_1$  is related to the gauge eigenstates through the rotation in Eq. (B.10). For decays to photons we are only sensitive to Goldstino interactions with the neutral gauginos, and we find

$$\Gamma_{\tilde{N}_1 \rightarrow \tilde{G} \gamma} = |R_{11}c_w + R_{21}s_w|^2 \frac{m_{\tilde{N}_1}^5}{48\pi m_{3/2}^2 M_{\text{Pl}}^2} . \quad (\text{B.26})$$

For decays to Z bosons, we have both longitudinal and transverse final states

$$\Gamma_{\tilde{N}_1 \rightarrow \tilde{G} Z_T} = |R_{11}s_w - R_{21}c_w|^2 \frac{m_{\tilde{N}_1}^5}{48\pi m_{3/2}^2 M_{\text{Pl}}^2} , \quad (\text{B.27})$$

$$\Gamma_{\tilde{N}_1 \rightarrow \tilde{G} Z_L} = |R_{41}s_\beta - R_{31}c_\beta|^2 \frac{m_{\tilde{N}_1}^5}{96\pi m_{3/2}^2 M_{\text{Pl}}^2} . \quad (\text{B.28})$$

Finally, for decays to Higgs bosons we have

$$\Gamma_{\tilde{N}_1 \rightarrow \tilde{G} h} = |R_{41}s_\beta + R_{31}c_\beta|^2 \frac{m_{\tilde{N}_1}^5}{96\pi m_{3/2}^2 M_{\text{Pl}}^2} , \quad (\text{B.29})$$

where we identify the SM-like Higgs boson  $h$  in the decoupling limit as in Eqs. (B.6) and (B.7)

---

<sup>5</sup>An important exception is when the main source for the soft masses is Anomaly Mediation [50, 51]. For the light gravitinos considered here, these corrections are very suppressed.



## C Free Streaming of Warm DM Component

Our framework provides a warm dark matter source through production of NLSP particles and subsequent decay  $\text{NLSP} \rightarrow \text{LSP } a$ , where  $a$  is a massless axion. We always assume that if the LSP is the gravitino (axino), then the NLSP is the axino (gravitino). In this Appendix, we provide the calculation of the free streaming length for such a warm component

$$\lambda_{\text{FS}} = \int_{\tau_{\text{NLSP}}}^{t_{\text{eq}}} \frac{v_{\text{LSP}}(t)}{a(t)} dt = \frac{2 t_{\text{eq}}}{a_{\text{eq}}^2} \int_{a_\tau}^{a_{\text{eq}}} v(a) da . \quad (\text{C.1})$$

Here,  $\tau_{\text{NLSP}}$  is the NLSP lifetime, whereas  $t_{\text{eq}}$  and  $a_{\text{eq}}$  are the time and scale factor at matter-radiation equality, respectively. In the second equality, we defined  $a_\tau = a(\tau_{\text{NLSP}})$  and we changed integration variable by using the relation for a radiation dominated universe  $a \propto t^{1/2}$ , justified if NLSP decays happen after BBN (i.e.  $\tau_{\text{NLSP}} \gtrsim 1 \text{ sec}$ ).

The LSP velocity  $v(a)$  after decays is just a consequence of free streaming. The initial energy and momentum at the decay time  $\tau_{\text{NLSP}}$  follow from four-momentum conservation

$$\{E_{\text{LSP}}^\tau, p_{\text{LSP}}^\tau\} = \{E_{\text{LSP}}(\tau_{\text{NLSP}}), p_{\text{LSP}}(\tau_{\text{NLSP}})\} = \left\{ \frac{m_{\text{NLSP}}^2 + m_{\text{LSP}}^2}{2m_{\text{NLSP}}}, \frac{m_{\text{NLSP}}^2 - m_{\text{LSP}}^2}{2m_{\text{NLSP}}} \right\} . \quad (\text{C.2})$$

The LSP momentum red-shifts with the Hubble expansion

$$v_{\text{LSP}}(a) = \frac{p_{\text{LSP}}(a)}{E_{\text{LSP}}(a)} = \left[ 1 + \left( \frac{m_{\text{LSP}}}{p_{\text{LSP}}^\tau} \frac{a}{a_\tau} \right)^2 \right]^{-\frac{1}{2}} , \quad (\text{C.3})$$

and the free streaming scale defined in Eq. (C.1) results in

$$\lambda_{\text{FS}} = 2 \frac{t_{\text{eq}}}{a_{\text{eq}}} \frac{p_{\text{LSP}}(a_{\text{eq}})}{m_{\text{LSP}}} [\mathcal{F}(a_{\text{eq}}) - \mathcal{F}(a_\tau)] , \quad (\text{C.4})$$

$$\mathcal{F}(a) = \log \left[ \frac{m_{\text{LSP}}}{p_{\text{LSP}}(a)} + \sqrt{1 + \left( \frac{m_{\text{LSP}}}{p_{\text{LSP}}^\tau} \frac{a}{a_\tau} \right)^2} \right] . \quad (\text{C.5})$$

It is convenient to derive an approximate expression for  $\lambda_{\text{FS}}$  by identifying the scale factor value  $a_{\text{NR}}$ , correspondent to the time when the free streaming LSP enters the non-relativistic regime. The LSP velocity in Eq. (C.3) can be approximated as follows

$$v(a) \simeq \begin{cases} 1 & a < a_{\text{NR}} \\ a_{\text{NR}}/a & a \geq a_{\text{NR}} \end{cases} . \quad (\text{C.6})$$

We find  $a_{\text{NR}}$  by imposing  $p_{\text{LSP}}(a_{\text{NR}}) \simeq m_{\text{LSP}}$  and we find  $a_{\text{NR}} \simeq a_\tau p_{\text{LSP}}^\tau / m_{\text{LSP}}$ . The free streaming length, as defined in Eq. (C.1), approximately reads

$$\lambda_{\text{FS}} \simeq \frac{2 t_{\text{eq}}}{a_{\text{eq}}} \frac{a_\tau}{a_{\text{eq}}} \frac{p_{\text{LSP}}^\tau}{m_{\text{LSP}}} \left[ 1 + \log \left( \frac{a_{\text{eq}}}{a_\tau} \frac{m_{\text{LSP}}}{p_{\text{LSP}}^\tau} \right) \right] . \quad (\text{C.7})$$

We evaluate this expression by using the known values  $t_{\text{eq}}/a_{\text{eq}} \simeq 93 \text{ Mpc}$ ,  $t_{\text{eq}} \simeq 2.2 \times 10^{12} \text{ sec}$ , and the time dependence of the scale factor  $a(t) = a_{\text{eq}}(t/t_{\text{eq}})^{1/2}$ . In the  $m_{\text{NLSP}} \gg m_{\text{LSP}}$  limit, the free streaming length reads

$$\lambda_{\text{FS}} \simeq 0.6 \text{ Mpc} \left( \frac{m_{\text{NLSP}}}{10 m_{\text{LSP}}} \right) \left( \frac{\tau_{\text{NLSP}}}{10^4 \text{ sec}} \right)^{1/2} \left[ 1 + 0.1 \log \left( \frac{10 m_{\text{LSP}}}{m_{\text{NLSP}}} \left( \frac{10^4 \text{ sec}}{\tau_{\text{NLSP}}} \right)^{1/2} \right) \right]. \quad (\text{C.8})$$

## References

- [1] R. D. Peccei and H. R. Quinn, Phys. Rev. Lett. **38**, 1440 (1977).
- [2] R. D. Peccei and H. R. Quinn, Phys. Rev. D **16**, 1791 (1977).
- [3] S. Weinberg, Phys. Rev. Lett. **40**, 223 (1978).
- [4] F. Wilczek, Phys. Rev. Lett. **40**, 279 (1978).
- [5] M. Dine, W. Fischler and M. Srednicki, Phys. Lett. B **104**, 199 (1981).
- [6] A. R. Zhitnitsky, Sov. J. Nucl. Phys. **31**, 260 (1980) [Yad. Fiz. **31**, 497 (1980)].
- [7] R. T. Co, F. D’Eramo, L. J. Hall and D. Pappadopulo, JCAP **1512**, no. 12, 024 (2015) [[arXiv:1506.07532](#) [hep-ph]].
- [8] L. J. Hall, K. Jedamzik, J. March-Russell and S. M. West, JHEP **1003**, 080 (2010) [[arXiv:0911.1120](#) [hep-ph]].
- [9] A. Strumia, JHEP **1006**, 036 (2010) [[arXiv:1003.5847](#) [hep-ph]].
- [10] V. S. Rychkov and A. Strumia, Phys. Rev. D **75**, 075011 (2007) [[hep-ph/0701104](#)].
- [11] K. J. Bae, K. Choi and S. H. Im, JHEP **1108**, 065 (2011) [[arXiv:1106.2452](#) [hep-ph]].
- [12] C. Cheung, G. Elor and L. J. Hall, Phys. Rev. D **85**, 015008 (2012) [[arXiv:1104.0692](#) [hep-ph]].
- [13] M. Hashimoto, K. I. Izawa, M. Yamaguchi and T. Yanagida, Phys. Lett. B **437**, 44 (1998) [[hep-ph/9803263](#)].
- [14] J. E. Kim, Phys. Rev. Lett. **43**, 103 (1979).
- [15] M. A. Shifman, A. I. Vainshtein and V. I. Zakharov, Nucl. Phys. B **166**, 493 (1980).
- [16] P. Graf and F. D. Steffen, JCAP **1312**, 047 (2013) [[arXiv:1302.2143](#) [hep-ph]].
- [17] D. J. H. Chung, E. W. Kolb and A. Riotto, Phys. Rev. D **60**, 063504 (1999) [[hep-ph/9809453](#)].

- [18] G. F. Giudice, E. W. Kolb and A. Riotto, Phys. Rev. D **64**, 023508 (2001) [[hep-ph/0005123](#)].
- [19] M. Kawasaki, T. Moroi and T. Yanagida, Phys. Lett. B **383**, 313 (1996) [[hep-ph/9510461](#)].
- [20] R. T. Co, F. D’Eramo and L. J. Hall, Phys. Rev. D **94**, no. 7, 075001 (2016) [[arXiv:1603.04439](#) [hep-ph]].
- [21] S. Dimopoulos, M. Dine, S. Raby and S. D. Thomas, Phys. Rev. Lett. **76**, 3494 (1996) [[hep-ph/9601367](#)].
- [22] S. P. Martin, Phys. Rev. D **62**, 095008 (2000) [[hep-ph/0005116](#)].
- [23] M. Kawasaki and K. Nakayama, Phys. Rev. D **77**, 123524 (2008) [[arXiv:0802.2487](#) [hep-ph]].
- [24] M. Kawasaki, N. Kitajima and K. Nakayama, Phys. Rev. D **83**, 123521 (2011) [[arXiv:1104.1262](#) [hep-ph]].
- [25] T. Asaka and T. Yanagida, Phys. Lett. B **494**, 297 (2000) [[hep-ph/0006211](#)].
- [26] H. Baer, S. Kraml, A. Lessa and S. Sekmen, JCAP **1104**, 039 (2011) [[arXiv:1012.3769](#) [hep-ph]].
- [27] H. Baer and A. Lessa, JHEP **1106**, 027 (2011) [[arXiv:1104.4807](#) [hep-ph]].
- [28] K. J. Bae, H. Baer, A. Lessa and H. Serce, JCAP **1410**, no. 10, 082 (2014) [[arXiv:1406.4138](#) [hep-ph]].
- [29] T. Moroi, H. Murayama and M. Yamaguchi, Phys. Lett. B **303**, 289 (1993). S. Weinberg, Phys. Rev. Lett. **48**, 1303 (1982). M. Y. Khlopov, A. D. Linde, Phys. Lett. **B138**, 265-268 (1984).
- [30] K. Jedamzik, Phys. Rev. D **70**, 063524 (2004) [[astro-ph/0402344](#)].
- [31] M. Kawasaki, K. Kohri and T. Moroi, Phys. Lett. B **625**, 7 (2005) [[astro-ph/0402490](#)].
- [32] J. R. Ellis, K. A. Olive and E. Vangioni, Phys. Lett. B **619**, 30 (2005) [[astro-ph/0503023](#)].
- [33] A. Boyarsky, J. Lesgourgues, O. Ruchayskiy and M. Viel, JCAP **0905**, 012 (2009) [[arXiv:0812.0010](#) [astro-ph]].
- [34] A. Harada and A. Kamada, JCAP **1601**, no. 01, 031 (2016) [[arXiv:1412.1592](#) [astro-ph.CO]].
- [35] A. Kamada, K. T. Inoue and T. Takahashi, Phys. Rev. D **94**, no. 2, 023522 (2016) [[arXiv:1604.01489](#) [astro-ph.CO]].
- [36] D. H. Weinberg, J. S. Bullock, F. Governato, R. Kuzio de Naray and A. H. G. Peter, Proc. Nat. Acad. Sci. **112**, 12249 (2014) [[arXiv:1306.0913](#) [astro-ph.CO]].

- [37] K. El-Badry, A. Wetzel, M. Geha , P. F. Hopkins, D. Kereš, T. K. Chan, C. A. Faucher-Giguère, *Astrophys. J.* **820**, 131 (2015), [[arXiv:1512.01235](#) [astro-ph.GA]]
- [38] A. R. Wetzel, P. F. Hopkins, J. h. Kim, C. A. Faucher-Giguere, D. Keres and E. Quataert, *Astrophys. J.* **827**, no. 2, L23 (2016) [[arXiv:1602.05957](#) [astro-ph.GA]].
- [39] K. A. Oman *et al.*, *Mon. Not. Roy. Astron. Soc.* **452**, no. 4, 3650 (2015) [[arXiv:1504.01437](#) [astro-ph.GA]].
- [40] E. Papastergis and F. Shankar, *A&A* 591, A58 (2016) [[arXiv:1511.08741](#) [astro-ph.GA]].
- [41] M. Kaplinghat, *Phys. Rev. D* **72**, 063510 (2005) [[astro-ph/0507300](#)].
- [42] J. A. R. Cembranos, J. L. Feng, A. Rajaraman and F. Takayama, *Phys. Rev. Lett.* **95**, 181301 (2005) [[hep-ph/0507150](#)].
- [43] C. Borschensky, M. Krmer, A. Kulesza, M. Mangano, S. Padhi, T. Plehn and X. Portell, *Eur. Phys. J. C* **74**, no. 12, 3174 (2014) [[arXiv:1407.5066](#) [hep-ph]].
- [44] J. P. Chou, D. Curtin and H. J. Lubatti, [arXiv:1606.06298](#) [hep-ph].
- [45] J. Tang *et al.*, [arXiv:1507.03224](#) [physics.acc-ph]. A. Ball, M. Benedikt, L. Bottura, O. Dominguez, F. Gianotti, B. Goddard, P. Lebrun, M. Mangano, D. Schulte, E. Shaposhnikova, R. Tomas, and F. Zimmermann (FCC-hh), Future Circular Collider Study Hadron Collider Parameters, Tech. Rep. (CERN, Geneva, 2014).
- [46] P. A. R. Ade *et al.* [Planck Collaboration], [arXiv:1502.01589](#) [astro-ph.CO].
- [47] K. N. Abazajian *et al.* [CMB-S4 Collaboration], [arXiv:1610.02743](#) [astro-ph.CO].
- [48] N. Arkani-Hamed, A. Delgado and G. F. Giudice, *Nucl. Phys. B* **741**, 108 (2006) [[hep-ph/0601041](#)].
- [49] E. Cremmer, S. Ferrara, L. Girardello and A. Van Proeyen, *Nucl. Phys. B* **212**, 413 (1983).
- [50] F. D’Eramo, J. Thaler and Z. Thomas, *JHEP* **1206**, 151 (2012) [[arXiv:1202.1280](#) [hep-ph]].
- [51] F. D’Eramo, J. Thaler and Z. Thomas, *JHEP* **1309**, 125 (2013) [[arXiv:1307.3251](#) [hep-ph]].
- [52] C. Cheung, Y. Nomura and J. Thaler, *JHEP* **1003**, 073 (2010) [[arXiv:1002.1967](#) [hep-ph]].
- [53] C. Cheung, F. D’Eramo and J. Thaler, *JHEP* **1108**, 115 (2011) [[arXiv:1104.2600](#) [hep-ph]].